Check for updates

Global Biogeochemical Cycles

RESEARCH ARTICLE
10.1029/2026GB009430

Drivers of Compound Marine Heatwaves and Acidity Extremes in the Southern Ocean

Joel Wong[1,2], **Matthias Münnich**[1], **and Nicolas Gruber**[1]

[1]Environmental Physics, Institute of Biogeochemistry and Pollutant Dynamics, ETH Zurich, Zürich, Switzerland, [2]Now at National Oceanography Centre, Southampton, UK

Key Points:

- Four types of column-compound extremes of Marine Heatwaves (MHW) and Ocean Acidity eXtremes (OAX) are identified in the Southern Ocean
- Surface MHW increase stratification and decrease productivity, driving co-occurring surface OAX through DIC retention and thermodynamics
- Subsurface co-occurring MHW and OAX are primarily caused by upwelling and advection of warm, acidic upper circumpolar deep waters

Supporting Information:

Supporting Information may be found in the online version of this article.

Correspondence to:

J. Wong,
joel.wong@noc.ac.uk

Citation:

Wong, J., Münnich, M., & Gruber, N. (2026). Drivers of compound marine heatwaves and acidity extremes in the Southern Ocean. *Global Biogeochemical Cycles*, *40*, e2026GB009430. https://doi.org/10.1029/2026GB009430

Received 13 JUL 2026
Accepted 15 OCT 2026

Author Contributions:

Conceptualization: Joel Wong, Matthias Münnich, Nicolas Gruber
Formal analysis: Joel Wong
Funding acquisition: Nicolas Gruber
Investigation: Joel Wong
Methodology: Joel Wong, Matthias Münnich, Nicolas Gruber
Resources: Matthias Münnich, Nicolas Gruber
Software: Joel Wong
Supervision: Matthias Münnich, Nicolas Gruber
Writing – original draft: Joel Wong
Writing – review & editing: Matthias Münnich, Nicolas Gruber

© 2026 The Author(s). Global Biogeochemical Cycles published by Wiley Periodicals LLC on behalf of American Geophysical Union.
This is an open access article under the terms of the Creative Commons Attribution License, which permits use, distribution and reproduction in any medium, provided the original work is properly cited.

Abstract Our previous work revealed that between 1980 and 2019, Column-Compound eXtremes (CCX) of Marine Heatwaves (MHW) and Ocean Acidity eXtremes (OAX) increased in frequency and intensity in the Southern Ocean (Wong et al., 2025, https://doi.org/10.1029/2025gb008630), disproportionately affecting the Antarctic zone and its Marine Protected Areas (MPAs). These extremes were identified using a fixed baseline in hindcast simulations with the Regional Ocean Modeling System (ROMS) coupled with the Biological Elemental Cycling (BEC) model. Extremes were classified as CCX when at least 50 m of each extreme was present in the upper 300 m. Here, we identify the driving processes of these CCX, using a detrended baseline to better separate these processes from the trend. We group these detrended CCX into four clusters, according to the locations of MHW and OAX within the water column. Surface CCX are primarily a response of MHW thermodynamically increasing acidity, with increased stratification reducing productivity. Subsurface CCX, particularly the most extreme ones around Antarctica, are mostly caused by the upwelling of warm and acidic Upper Circumpolar Deep Water. The CCX characterized by surface MHW and subsurface OAX tend to be initiated by MHW, which stimulates higher productivity and export, thereby enhancing remineralization at depth. The occurrence of these clusters is modulated interannually by large-scale climate variability that influences Ekman divergence and upper-ocean stratification. Improving our understanding of the links between large-scale climate variability and local CCX processes provides a foundation for improving the predictability of CCX and assessing their potential impact on marine ecosystems, particularly within MPAs.

Plain Language Summary Between 1980 and 2019, vertically compounded Marine Heat Waves (MHW) and Ocean Acidity eXtremes (OAX) became more frequent and intense in the Southern Ocean, especially near Antarctica and within its Marine Protected Areas. These "Column-Compound eXtremes" (CCX) were identified in our previous study (Wong et al., 2025, https://doi.org/10.1029/2025gb008630) using an ocean-biogeochemical model. This study continues this work to determine the drivers behind these CCX. First, we identified four main types of compound extremes based on where extremely warm and acidic waters occur in the water column. Surface CCX are mainly caused by warmer temperatures directly increasing ocean acidity, while stronger stratification reduces biological productivity. Subsurface CCX, including the strongest events around Antarctica, are primarily a result of the upwelling of warm, acidic deep waters. In some cases, MHW increase biological production at the surface, leading to greater sinking organic matter and enhanced remineralization at depth, which causes subsurface acidity extremes. We also found that large-scale climate variability influences how often these different types of CCX occur by altering ocean circulation, stratification, and sea ice conditions. Understanding these mechanisms improves our ability to predict future compound extremes and assess their impacts on Southern Ocean ecosystems.

1. Introduction

Marine Heat Waves (MHW) and other extremes have captured the attention of scientists and the public alike, mainly due to the threat they pose to marine organisms and ecosystems (Gomes et al., 2024; Gruber et al., 2021; Guibourd de Luzinais et al., 2024; Smith, 2025). Although the majority of the research has focused on surface extremes, there is rapidly growing interest in understanding sub-surface and biogeochemical extremes (Kohlman et al., 2025; Köhn et al., 2024; Le Grix et al., 2025; Malan et al., 2025; Zhang et al., 2023). Wong et al. (2024) introduced the concept of Column-Compound eXtremes (CCX), which occur when at least 50 m of two different extremes occur within the upper 300 m of the water column. CCX have the potential to disrupt the habitat of marine organisms that migrate within the upper water column and have been increasing in frequency and intensity under climate change.

19449224, 2026, 10, Downloaded from https://agupubs.onlinelibrary.wiley.com/doi/10.1029/2026GB009430 by Catherine Becker - University Of Southampton , Wiley Online Library on [11/11/2026]. See the Terms and Conditions (https://onlinelibrary.wiley.com/terms-and-conditions) on Wiley Online Library for rules of use; OA articles are governed by the applicable Creative Commons License

In Wong et al. (2025), using model simulations and a fixed baseline to identify extremes, we showed that CCX have become more frequent and intense in the Southern Ocean, occupying an increasing fraction of the water column. Between 1980 and 2019, the Antarctic zone experienced the strongest changes, with increases of up to 180 CCX days per year, 120 days in duration, and −0.2 pH in OAX intensity, driven by long trends in ocean temperature and acidity. These shifts reduce the availability of habitable space in the epipelagic zone and pose increasing risks to marine organisms. They are particularly acute in existing and proposed Antarctic Marine Protected Areas (MPAs), with the Ross Sea and Antarctic Peninsula MPAs disproportionately affected relative to the surrounding Antarctic zone. Moreover, the vertical extent of CCX varies by latitude: while MHW in the Northern zone remain largely confined to the surface, CCX in the Subantarctic and Antarctic often span the full water column, with subsurface layers experiencing especially intense OAX.

The growing occurrence and ecological risks of CCX in the Southern Ocean highlight the need to identify their driving mechanisms. The identification of these processes, which are driven by local marine and atmospheric weather patterns, is obscured by the long-term trends in ocean warming and acidification. These trends strongly increase the likelihood for extreme conditions to occur, whereas the actual processes driving the extremes tend to remain the same. Thus, in order to focus on the role of local drivers causing extremes, we analyse extremes on a detrended baseline, that is, where long-term trends are removed (Smith, 2025; Wong et al., 2025).

Local processes that can push ocean temperatures and ocean acidity above their natural variability include physical processes such as surface fluxes, vertical mixing and vertical and horizontal advection, as well as biological processes such as primary production and remineralization (Fernández-Barba et al., 2024; Leseurre et al., 2022; Wilson et al., 2019). These processes can be triggered through remote changes, such as in winds that affect ocean circulation and mixing, or in the extent of sea ice that can affect the large-scale exchange of heat and carbon (Eayrs et al., 2021; G. Wang et al., 2022). Identifying the conditions that cause CCX is critical to assess how these events emerge from observable changes in sea ice, winds, and sea surface temperatures. Skilled predictions in these drivers therefore have the potential to predict CCX and its resulting biological implications. In addition, linking CCX to their physical and biogeochemical drivers provides insight into the risks they pose to marine organisms. For example, anomalously low sea ice can not only lead to extreme events but can also disrupt the recruitment of sympagic grazers, that is, grazers associated with sea ice (Lowe et al., 2012; Quetin & Ross, 2009).

In the Southern Ocean, Fernández-Barba et al. (2024) identified air–sea heat exchange and horizontal heat advection as the dominant drivers of surface MHW, while vertical mixing generally acted to dampen MHW, consistent with global patterns reported by Burger and Frölicher (2023). In contrast, OAX tends to driven by vertical mixing and changes in primary production, export, and subsequent remineralization, affecting acidity from the surface down deep into the water column. Some of these biological changes can be related to MHW, as described by Fernández-Barba et al. (2024), who observed enhanced primary production in subantarctic regions during surface MHW. Another process that can lead to co-occurring MHW and OAX, particularly at depth, is the vertical displacement of the pycnocline, associated, for example, with the upwelling or downwelling of warm, acidic waters (Le Grix et al., 2025). Together, these studies underscore the dynamic, depth-dependent, and multi-process nature of extreme events in the Southern Ocean. However, important gaps remain: no study has systematically investigated the drivers of MHW and OAX that occur simultaneously in different parts of the water column, nor explicitly assessed the role of biological production and carbon export in driving OAX. Addressing these gaps, this study examines how local physical and biogeochemical conditions throughout the vertical column drive the occurrence of CCX.

The attribution of surface and subsurface MHW drivers has relied on a range of approaches. Statistical methods, such as associations with climate modes (Holbrook et al., 2019; Wong et al., 2025) and composite analyses (Schaeffer & Roughan, 2017; A. Sen Gupta et al., 2020) that link extremes to shifts in large-scale variability, have been employed. Process-based approaches, including mixed-layer heat budget analyses (Bian et al., 2023; Elzahaby et al., 2021; Richaud et al., 2024), were used to directly quantify contributions from air–sea fluxes, advection, and mixing. For OAX, driver attribution has been achieved through decomposition of daily $[H^+]$ tendencies into local contributions from temperature (T), dissolved inorganic carbon (DIC), and total alkalinity (Alk) using circulation models (Burger & Frölicher, 2023; Wong et al., 2025). Together, these methodologies span scales from basin-wide climate variability to local flux processes, offering complementary perspectives on the emergence of extremes. However, most studies examined the drivers of MHW or OAX in isolation and are

19449224, 2026, 10, Downloaded from https://agupubs.onlinelibrary.wiley.com/doi/10.1029/2026GB009430 by Catherine Becker - University Of Southampton , Wiley Online Library on [11/11/2026]. See the Terms and Conditions (https://onlinelibrary.wiley.com/terms-and-conditions) on Wiley Online Library for rules of use; OA articles are governed by the applicable Creative Commons License

typically confined to the surface or a single depth level, leaving the drivers of CCX across the water column unresolved.

Here, we address these gaps by identifying the physical and biogeochemical drivers of the CCX events in the Southern Ocean described by Wong et al. (2025). We classify the CCX they detected on a detrended baseline according to the vertical location of MHW and OAX within the water column, yielding four distinct clusters. Driver attribution is performed for each cluster using a hierarchical approach. We first link the events to their local drivers and potential remote drivers, such as the Southern Annular Mode (SAM). We then constrain the temperature and dissolved inorganic carbon (DIC) budgets to attribute daily changes to local physical and biogeochemical fluxes, directly identifying the processes driving MHW and OAX. Finally, we synthesize both statistical and flux-based analyses to construct the process chain underlying the onset of CCX. In doing so, we identify not only the drivers of MHW and OAX individually, but also the shared mechanisms that lead to their co-occurrence within the water column.

2. Methods

This study makes use of the model simulations and CCX analyses of Wong et al. (2025). In the following, we first summarize the simulations, then reiterate the definitions of CCX and finally describe the clustering and the analyses of the tendencies.

2.1. ROMS-BEC Model Hindcast

The historical conditions of the Southern Ocean are simulated between 1980 and 2019 using the UCLA-ETHZ version of the Regional Ocean Modeling System (ROMS, Shchepetkin and McWilliams (2005)), coupled with the Biological Elemental Cycling (BEC, Moore et al. (2013)) model. The model was set up with a horizontal resolution of 25° and 64 terrain following depth levels, simulating the ocean between the Antarctic continent and 24°S. It is run with the forcing of wind and the fluxes of heat and freshwater derived from the ERA5 reanalysis (Wong et al., 2025). For further details, especially with regard to the treatment of freshwater fluxes, we refer to Wong et al. (2025) as well as to Hague et al. (2024) and Haumann et al. (2016). Here, we use exactly the same model output as Wong et al. (2025), confining our analysis to the Southern Ocean between 40°S and 78°S. We divide the analysis region into the Northern, Subantarctic, and Antarctic zones of the Marine Ecosystem Assessment of the Southern Ocean, which form the basis of planning MPAs (Constable et al., 2023).

As Wong et al. (2025), we applied drift and bias corrections to the model output prior to our analyses of the extremes. Specifically, model potential temperature was first corrected for drift before being used to detect MHWs. Similarly, model DIC and Alk were first corrected for drift and subsequently bias-corrected against the Global Ocean Data Analysis Project Version 2 climatology (GLODAPv2, Lauvset et al. (2016)), before being used to compute $[H^+]$. Concretely, we determined a mean annual bias for each grid cell for both DIC and Alk compared to the GLODAPv2 reference year of 2002. We then applied this offset correction for all times (Text S1 in Supporting Information S1) Finally, $[H^+]$ is then calculated using MOCSY 2.0 (Orr & Epitalon, 2015) from the corrected temperature, DIC, and Alk, together with salinity and the concentrations of phosphate and silicate.

A limitation concerns the treatment of sea-ice freshwater fluxes. These fluxes were constructed by adding a climatological forcing to observation-based linear trends from 1980 to 2008, which were then held constant thereafter. Nevertheless, sea-ice concentration varies interannually according to observations, continuing to influence local and remote variability through its modulation of heat and momentum fluxes (Hague et al., 2024).

2.2. Extreme Event Definitions

We used the definition of CCX by Wong et al. (2024) to study compounded MHW and OAX. First, the underlying MHW and OAX were detected using a detrended baseline (Smith, 2025). We adopted this approach in order to better isolate the underlying drivers, as long-term trends tend to obscure the specific conditions required to push the system into an extreme state. This is supported by Jacox (2019) and Oliver et al. (2021), who pointed out that detrended baselines are an appropriate choice for the study of drivers and mechanisms, as extreme events are defined relative to the conditions of the time period in which they occur.

To achieve this detrending, the model simulated temperature (T) and hydrogen ion concentration ($[H^+]$) were first fit at each grid cell and depth level of the model with a quadratic trend. These trends were then removed, thus

19449224, 2026, 10, Downloaded from https://agupubs.onlinelibrary.wiley.com/doi/10.1029/2026GB009430 by Catherine Becker - University Of Southampton , Wiley Online Library on [11/11/2026]. See the Terms and Conditions (https://onlinelibrary.wiley.com/terms-and-conditions) on Wiley Online Library for rules of use; OA articles are governed by the applicable Creative Commons License

adjusting the values to the baseline year of 1980. The daily thresholds for MHW and OAX were then determined from the detrended data by taking the 95th percentile of T or $[H^+]$ over an 11-day moving window centered on each day of the year (Hobday et al., 2016). Finally, MHW and OAX were detected for each grid cell individually by comparing the detrended values with the thresholds.

Switching perspectives to the water column, we analyzed MHW and OAX throughout the upper 300 m of the water column to identify Column-Single eXtremes (CSX) and CCX. Specifically, CSX require at least 50 m of the upper 300 m water column to be extreme in a single variable. A CCX occurs when CSX in MHW and in OAX overlap in time and horizontal grid cell, regardless of the vertical locations of the extremes (Wong et al., 2025). Following the MHW definition of Hobday et al. (2016), we retain only CCX events that last at least 5 days. This criterion also ensures that the events analyzed are sufficiently persistent for driver attribution.

We analyze the drivers of the extremes during their onset, which we define as the period from the start of the CCX until the day of the events' maximum intensity (Burger & Frölicher, 2023). When considering the local fluxes as drivers of CCX, we additionally analyze the build-up phase, that is, the days before the start of the CCX when the associated variables exceed the 68th percentile. The build-up phase is limited to a maximum of 20 days.

2.3. Clustering of CCX

To classify CCX based on the vertical structure of the constituent extremes, we use a k-means clustering algorithm (MacQueen, 1967). Clustering is performed on CCX events using the vertical locations of the single extremes constituting each event. Specifically, the number of MHW and OAX days each at every depth level for the duration of each CCX event is summed and then normalized by the duration of the CCX event. Then a principal components analysis is performed on the depth dimension, reducing the number of predictors from 58 (T and $[H^+]$ at 29 depth levels) to 15, while accounting for 96% of their variance. Finally, K-means clustering is performed with these 15 predictors, clustering the CCX events into four distinct clusters. In contrast to the clustering methodology used by Wong et al. (2024), where all events within the grid cell were summed, every CCX event is used as a clustering sample in this study. Compared to the global study by Wong et al. (2024), the Southern Ocean hindcast of this study captures finer-scale physical processes in a highly dynamic Southern Ocean. Thus, clustering by event enables the characterization of multiple types of CCX at the same location, allowing for the analysis of different processes that lead to distinct types of CCX at the same location. More details on the clustering methodology and choice of the number of clusters can be found in Text S2 of the Supporting Information S1.

2.4. Decomposition of the $[H^+]$ Anomaly

$[H^+]$ is influenced by a combination of factors, including T, DIC, Alk, salinity, and the concentration of minor acids. We quantify the dominant contributors to the $[H^+]$ anomalies during the onset of OAX events within a CCX event using a first order Taylor expansion (Burger & Frölicher, 2023):

$$\Delta[H^+] = \frac{\partial[H^+]}{\partial T}\Delta T + \frac{\partial[H^+]}{\partial DIC}\Delta sDIC + \frac{\partial[H^+]}{\partial Alk}\Delta sAlk + \dots, \quad (1)$$

where ΔT, $\Delta sDIC$, and $\Delta sAlk$ represent daily anomalies in temperature, salinity normalized DIC, and salinity normalized Alk from their climatological values. The partial derivatives are calculated for each day of the year from the hindcast climatological mean, using MOCSY 2.0 (Orr & Epitalon, 2015). Salinity-normalized DIC and Alk were used to remove the effect of freshwater dilution and concentration on biologically and physically driven changes in DIC and Alk (Text S1 in Supporting Information S1; Lovenduski et al. (2007)). The Taylor expansion was then evaluated using the sensitivities of $[H^+]$ to temperature, DIC, alkalinity, and salinity calculated with MOCSY 2.0. Because the salinity in the study domain remains close to the reference salinity of 35 g/kg, using MOCSY sensitivities with salinity-normalized DIC and Alk introduces only a small error (typically $<5\%$). The salinity contributions, together with the contributions from silicate and phosphate, were excluded from the subsequent analyses because these terms are expected to be much smaller than the dominant temperature, DIC and alkalinity contributions. Each term was computed during the onset period of OAX within each CCX, defined as the interval from the start of the CCX until the day of the highest column-maximum OAX intensity. Details of the decomposition of $[H^+]$ and the use of MOCSY 2.0 can be found in Text S1 of the Supporting Information S1.

19449224, 2026, 10, Downloaded from https://agupubs.onlinelibrary.wiley.com/doi/10.1029/2026GB009430 by Catherine Becker - University Of Southampton , Wiley Online Library on [11/11/2026]. See the Terms and Conditions (https://onlinelibrary.wiley.com/terms-and-conditions) on Wiley Online Library for rules of use; OA articles are governed by the applicable Creative Commons License

2.5. Local Tendencies of Temperature and DIC

To diagnose the drivers of MHW and OAX, we analyze the daily tendencies of T and DIC that contribute to their development. Changes in T can contribute to both MHW and OAX while changes in DIC affect only OAX (Equation 1). We also quantify anomalies in the daily tendencies of T and DIC. These analyses are restricted to grid cells that experience an MHW or OAX during a CCX event.

Specifically, the change in the daily average temperature (ΔT) between each day is decomposed into the following components:

$$\Delta T \simeq \Delta T^{\mathrm{as}} + \Delta T^{\mathrm{ah}} + \Delta T^{\mathrm{av}} + \Delta T^{\mathrm{mix}}, \tag{2}$$

where ΔT^{as} represents the temperature tendency resulting from air-sea heat exchange, ΔT^{ah} and ΔT^{av} represent horizontal and vertical heat advection, respectively, and ΔT^{mix} combines heat transport by local mixing, vertical diffusion, vertical convective mixing, and other minor processes.

Similarly, the daily average change in DIC (ΔC) is decomposed as follows:

$$\Delta C \simeq \Delta C^{\mathrm{as}} + \Delta C^{\mathrm{phys}} + \Delta C^{\mathrm{prod}} + \Delta C^{\mathrm{remin}} + \Delta C^{\mathrm{minor}}, \tag{3}$$

where ΔC^{as} represents the tendency of DIC due to the exchange of CO_2 with the surface, ΔC^{phys} represents the tendencies of DIC of advective, mixing, diffusive, convective, and other minor physical processes, ΔC^{prod} represents the drawdown of DIC due to net primary production and $\Delta C^{\mathrm{remin}}$ represents the increase in DIC from the remineralization of sinking particulate organic carbon (POC), and $\Delta C^{\mathrm{minor}}$ represent other minor terms relating to the remineralization of dissolved organic carbon and calcium carbonate dissolution.

The model archives surface and advective DIC tendencies separately but does not archive mixing and several smaller tendency terms individually. Therefore, we define a residual term that, together with the advective tendency, represents the net effect of physical transport on DIC $\left(\Delta C^{\mathrm{adv+res}}\right)$. This residual mainly comprises unresolved mixing, diffusion, and convection, but also includes the comparatively small biogeochemical terms of $\Delta C^{\mathrm{minor}}$ (Lovecchio et al., 2023; Sun & Ellwood, 2025). Combining these terms is appropriate for the present analysis because advective and mixing tendencies exhibit strong local compensation, such that their net contribution provides a more meaningful measure of physical transport than either term alone.

We also repeat this analysis for the anomalies in the daily T and DIC tendencies during CCX. This allows us to further isolate the fluxes responsible for driving extreme temperature and $[H^+]$. In practice, the daily climatology of each tendency term is calculated during an 11-day moving window, similar to the calculation of temperature and $[H^+]$ climatologies. The anomalies are then determined by taking the difference between each daily value with its climatological value, resulting in de-seasonalized anomalies of the contributions. Finally, these anomalies are expressed as a fraction of the daily T and DIC tendencies. This enables us to compare anomalies in tendencies regardless of location or season within each cluster.

Note that we adopted a local Eulerian framework in this tendency analysis. Therefore, it does not trace the physical origin of temperature or DIC in the Lagrangian sense (Eisbrenner, 2025). Consequently, heat acquired through surface fluxes on a given day and advected into another grid cell on subsequent days is attributed to advective processes when it contributes to the onset of CCX.

2.6. Composite Analysis of CCX Events During ENSO and SAM

We employ a composite analysis to investigate the relationships between the occurrence of CCX events and the large-scale climate pattern, that is, the El Niño/Southern Oscillation (ENSO) and the Southern Annular Mode (SAM) (Godoi & Torres Júnior, 2020; J. Wang et al., 2023). We thereby quantify the fraction of CCX area during each combination of modes relative to a neutral phase.

To classify each month of the hindcast into ENSO and SAM modes, we computed the Oceanic Niño Index (ONI, NOAA (n.d.)) and the Antarctic Oscillation Index (AOI, Gong and Wang (1999)) using the model's forcing fields from the ECMWF Reanalysis 5 (Hersbach et al., 2020). Specifically, the mean sea surface temperature in the Niño

19449224, 2026, 10, Downloaded from https://agupubs.onlinelibrary.wiley.com/doi/10.1029/2026GB009430 by Catherine Becker - University Of Southampton , Wiley Online Library on [11/11/2026]. See the Terms and Conditions (https://onlinelibrary.wiley.com/terms-and-conditions) on Wiley Online Library for rules of use; OA articles are governed by the applicable Creative Commons License

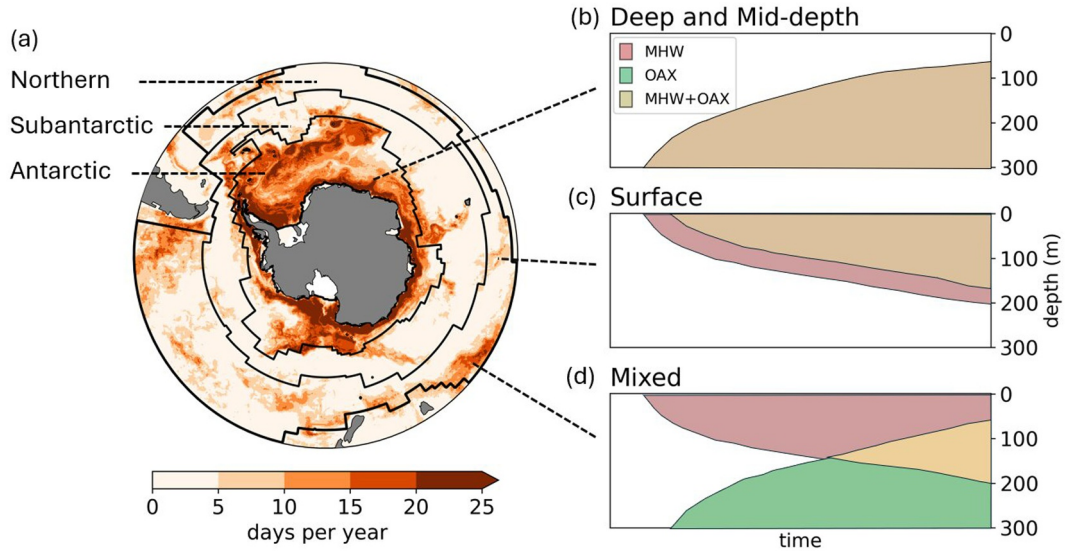


Figure 1. Mean frequency and representative vertical structures of CCX in the Southern Ocean over the simulation period (1980 through 2019). CCX are analyzed on a detrended baseline, adjusted to 1980. (a) Mean number of CCX days per year and boundaries of the Marine Ecosystem Assessment for the Southern Ocean regions. Right panels: Schematics of the typical time-depth evolution of CCX found at (b) Deep and Mid-depths, (c) Surface, and (d) Mixed depths of the top 300 m of the water column.

3.4 region and the zonal mean sea level pressure at 40°S and at 60°S are used. A detailed methodology for calculating these indices and determining positive and negative modes can be found in Text S3 of the Supporting Information S1. The hindcast contains between 30 and 81 months of various combinations of ENSO and SAM modes, while 100 months are classified as neutral (Figure S1 in Supporting Information S1).

The composite analysis is conducted on a monthly time scale as the dynamic response of the ocean to SAM is essentially immediate (A. S. Sen Gupta & England, 2006), while the timescale of atmospheric ENSO teleconnections to the Southern Ocean is on the order of weeks to months (L'Heureux & Thompson, 2006; G. Wang et al., 2022). To bridge this difference in timescales, we rely on the 3-month running mean and 5-month minimum duration applied to ONI for the classification of positive and negative ENSO events.

The writing process for this manuscript was supported by the artificial intelligence tools *Writefull* and *ChatGPT*.

3. Results

CCX on a detrended baseline are predominantly found in the Antarctic zone (Figure 1a). There, CCX are quite prevalent, occurring more than 20 days per year over the hindcast period. In contrast, CCX are rare over broad regions of the Southern Ocean, especially in the Subantarctic and Northern zones, with frequencies of less than 5 days per year. In the subsequent section, we show that the vertical structures of these events differ substantially between the different regions. Near Antarctica, CCX are typically characterized by both MHW and OAX occurring in the lower parts of the water column, that is, below 150 m (Figure 1b). In the Subantarctic and the Northern zones, MHW and OAX typically co-occur near the surface (Figure 1c). However, we also find mixed CCX events in these regions, that is, with MHW on the surface and OAX in the subsurface (Figure 1d).

3.1. Vertical Structure and Characteristics of CCX Clusters

The four clusters identified by the k-means clustering approach have distinct vertical structures in the upper 300 m (Figure 2). In the first three clusters, MHW and OAX co-occur at similar depths (Figure 2a), from having a surface expression (cluster 3), to mid-depths (cluster 2), or deeper in the 300 m deep column (cluster 1). In contrast, the depth structure of cluster 4 differs between MHW and OAX, with MHW occurring near the surface and OAX occurring in the subsurface below, that is, around 100 m. We subsequently refer to cluster 1 as "Deep" (C1), cluster 2 as "Mid-depth" (C2), cluster 3 as "Surface" (C3), and cluster 4 as "Mixed" (C4). The occurrence of events in each cluster and zone also shows spatial (Figures 2b and 2c) and seasonal (Figure 2d) differences.

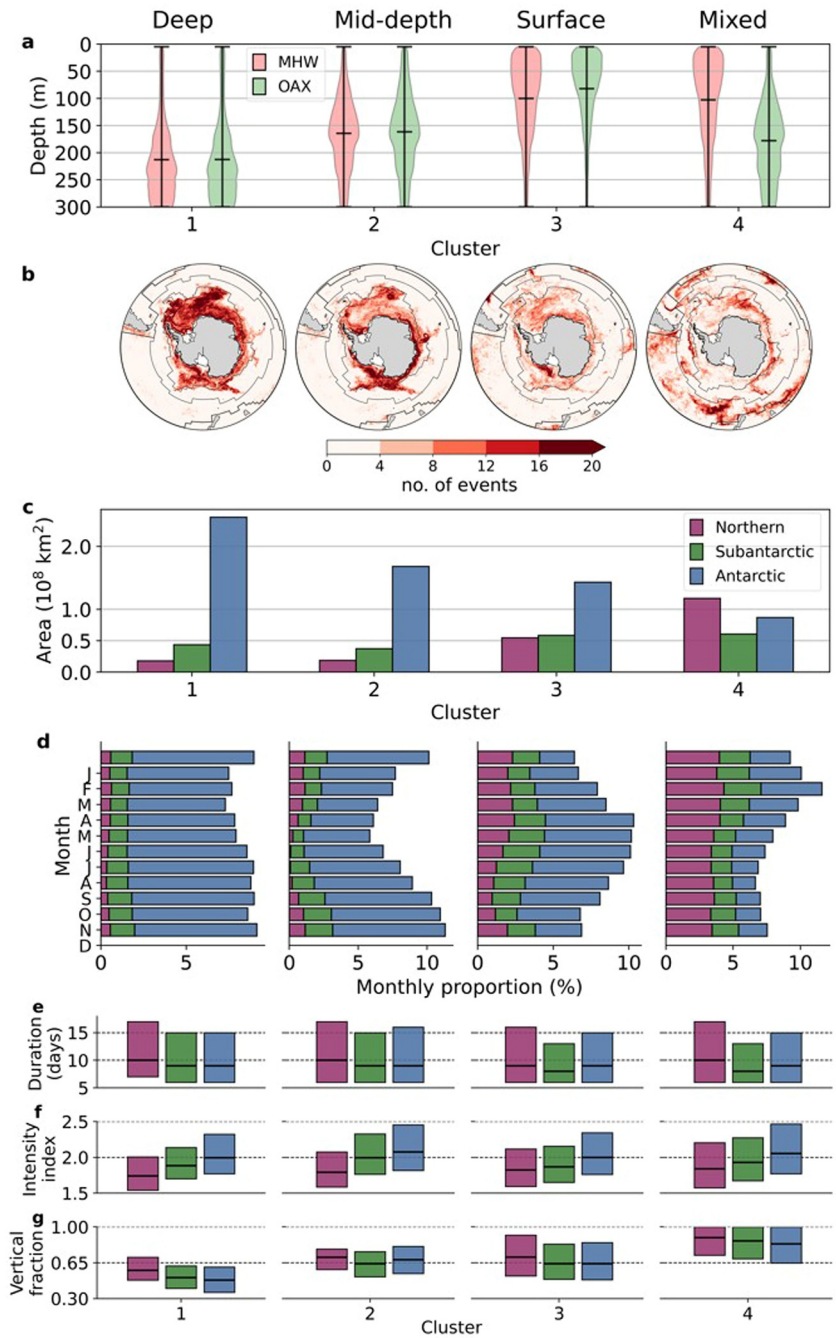


Figure 2. Properties of the detrended CCX events in the four selected clusters, further separated into the Marine Ecosystem Assessment for the Southern Ocean zones. (a) Relative distribution of MHW and OAX at each depth level, (b) spatial distribution of CCX events during the hindcast period, (c) cumulative daily area of CCX events, (d) monthly proportion of total CCX area within each cluster, and the median and interquartile range of CCX event (e) duration, (f) maximum intensity index, and (g) vertical fraction occupied by extremes.

Furthermore, CCX in these clusters also differ in duration, intensity, and vertical fraction of the column occupied by extremes (Figure 2e).

Deep CCX (C1) with MHW and OAX co-occurring below 150 m are the most dominant cluster in the Southern Ocean, making up 29% of all CCX. They are found predominantly in the Antarctic zone, where they are also the most frequently occurring cluster (Figure 2c). Deep CCX vary little seasonally and are reminiscent of the deep

19449224, 2026, 10, Downloaded from https://agupubs.onlinelibrary.wiley.com/doi/10.1029/2026GB009430 by Catherine Becker - University Of Southampton , Wiley Online Library on [11/11/2026]. See the Terms and Conditions (https://onlinelibrary.wiley.com/terms-and-conditions) on Wiley Online Library for rules of use; OA articles are governed by the applicable Creative Commons License

19449224, 2026, 10, Downloaded from https://agupubs.onlinelibrary.wiley.com/doi/10.1029/2026GB009430 by Catherine Becker - University Of Southampton , Wiley Online Library on [11/11/2026]. See the Terms and Conditions (https://onlinelibrary.wiley.com/terms-and-conditions) on Wiley Online Library for rules of use; OA articles are governed by the applicable Creative Commons License

MHW described in Wong et al. (2025) near the Antarctic continent. These events are found in the marginal ice zone (Figure 2b), with many areas experiencing more than 20 events during the hindcast period. In contrast, deep CCX are much less common in the Northern and Subantarctic zones.

Mid-depth CCX (C2) occur in regions similar to those of deep CCX. These events are also most frequent in the Antarctic Zone, but with a stronger occurrence during austral summer, corresponding to the period of sea ice melt (Figures 2b–2d).

Surface CCX (C3) occur relatively more frequently in the Northern and Subantarctic zones, although they still account for a large fraction of extremes in the Antarctic Zone (Figure 2c). In the Northern Zone, they are found primarily near the northern edge of the domain toward the subtropics. In the Antarctic Zone, they occur frequently close to the Antarctic continent, with a strong preference for austral winter and the period of sea ice formation (Figures 2b–2d).

Mixed CCX (C4) frequently co-occur in the Northern Zone and evenly throughout the year. These events tend to occur along strong frontal currents that are also regions of elevated productivity. In the Antarctic Zone, they occur more frequently at the edge of the marginal ice zone during the period of minimum sea ice extent and enhanced primary production. As MHW and OAX occur in different parts of the water column, extremes occupy the largest vertical fraction in Mixed CCX (Figure 2g).

3.2. Temporal Variability of CCX Clusters

The annual mean of daily CCX area reveals distinct decadal variability in all clusters (Figures 3a–3d). In particular, CCX occurrence was higher between 1985 and 1994, decreased between 1995 and 2014, and increased again after 2015. Based on these broad changes, we divide the hindcast period by visual inspection into four periods of low (1980–1984), high (1985–1994), low (1995–2014), and high (2015–2019) CCX area, with mean annual daily CCX areas of (8, 16, 6, and 10) $\times 10^5$ km^2, respectively. The same periods are applied across clusters to facilitate comparison of their environmental conditions, and are intended to capture broad differences in CCX occurrence rather than define distinct climatic regimes. The alternating pattern is also reflected in anomalies in the mean state of the Southern Ocean, including northward transport, pycnocline depth, NPP, POC export, and sea ice concentration (Figures 3h–3l).

Low sea ice concentration may result from increased westerly wind stress and upwelling of warm and acidic deep waters (Lee et al., 2017), potentially favoring the co-occurrence of MHW and OAX. Sea ice anomalies may also influence CCX directly by modulating surface heat and momentum fluxes (Delille et al., 2014; Loose & Schlosser, 2011), or indirectly through shifts in the position of the westerly wind belt that perturb the pycnocline and northward transport of surface waters (Figures 3h and 3i; Ramadhan et al. (2022)). Consistent with these potential mechanisms, we find significant rank correlations between annual total sea ice area and CCX occurrence across all zones (R = 0.50–0.67). We also find enhanced NPP and POC export during the high-CCX periods, indicating that decadal variability in the physical state of the Southern Ocean is accompanied by changes in its biological state. The biogeochemical mechanisms underlying these changes are examined in later sections.

These decadal shifts in the state of the Southern Ocean suggest that CCX may become more frequent or prolonged during these periods, contributing to the variability seen on interannual timescales. These periodic anomalies offer preliminary insight into the potential drivers of MHW and OAX, but allow only broad conjectures, as the response of CCX may vary across sectors within each zone. The following sections aim to establish direct links between physical and biogeochemical processes and CCX that occur at different depths. Although surface MHW have been shown to correlate with ENSO and SAM in the Southern Ocean (Holbrook et al., 2019; A. Sen Gupta et al., 2020), our analysis did not reveal a significant interannual or monthly correlation between zonal mean CCX days per year with ONI or AOI, up to a lag time of 6 months. This remains true even when the analysis is restricted to strong events (ONI and AOI thresholds of ±1). This aligns with the findings of Wong et al. (2025), who reported a weak relationship between CCX and ENSO in the Southern Ocean. However, this does not exclude ENSO and SAM as potential drivers of CCX, as their effects may still manifest on zonal and seasonal scales.

3.3. Physical and Biogeochemical Anomalies During CCX

We further examine changes in environmental states during CCX by quantifying the anomalies of physical and biogeochemical state variables during CCX (Figure 4). A description of these variables can be found in Text S4 of

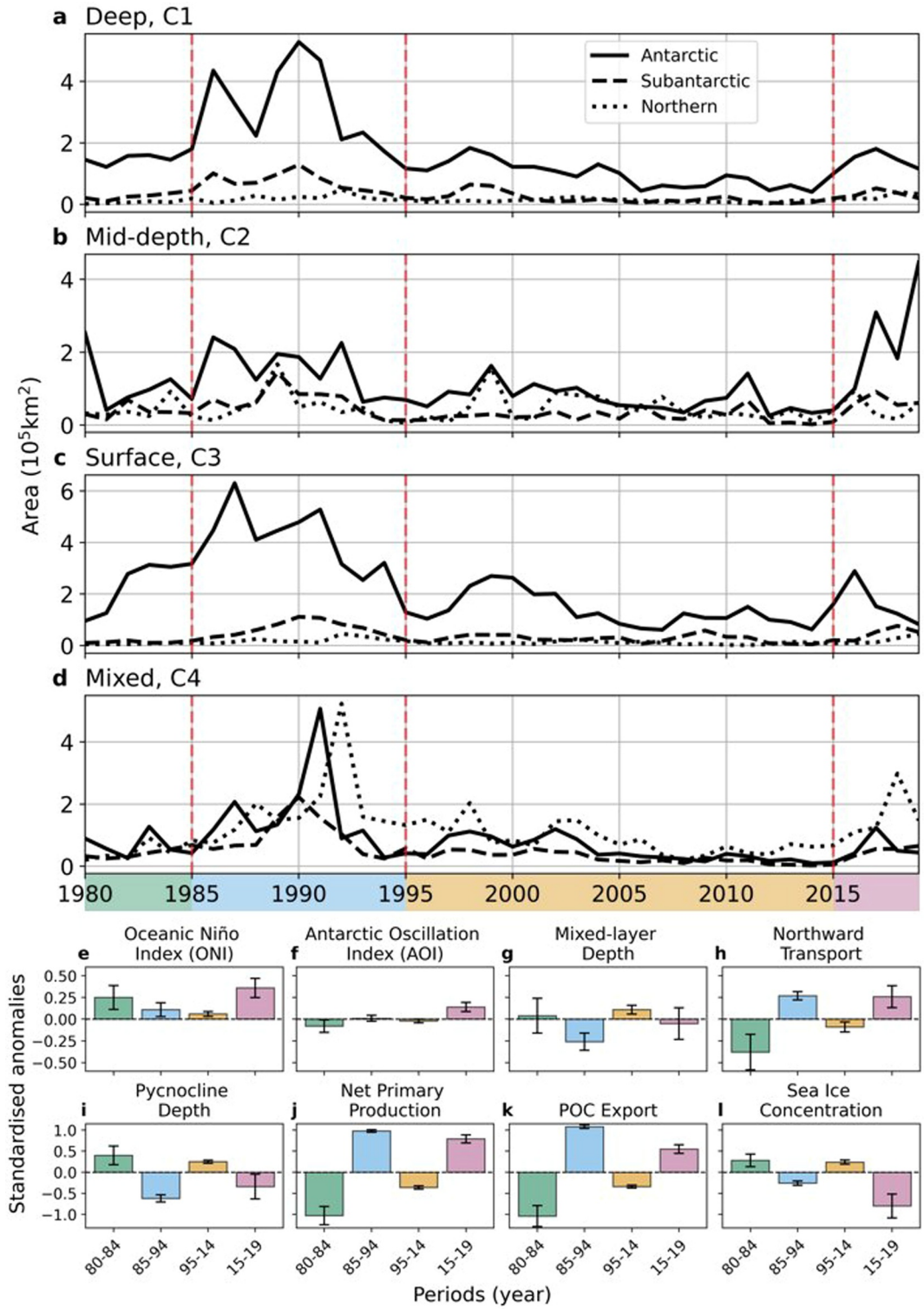


Figure 3. Interannual variability of CCX events in each cluster on a detrended baseline. Annual mean daily CCX area of (a) Deep (C1), (b) Mid-depth (C2), (c) Surface (C3), (d) Mixed (C4) events, and the period-mean standardized anomalies in the variables of the (e) Oceanic Niño index (ONI), (f) Antarctic Oscillation Index, (g) mixed-layer depth, (h) northward surface transport at 50−60°S (i) pycnocline depth, (j) net primary production, (k) particulate organic carbon export at 100 m depth, and (l) sea ice concentration. The periods are denoted by red dotted lines in (a) to (d). Error bars in (e–l) show the standard error for each period.

19449224, 2026, 10, Downloaded from https://agupubs.onlinelibrary.wiley.com/doi/10.1029/2026GB009430 by Catherine Becken - University Of Southampton , Wiley Online Library on [11/11/2026]. See the Terms and Conditions (https://onlinelibrary.wiley.com/terms-and-conditions) on Wiley Online Library for rules of use; OA articles are governed by the applicable Creative Commons License

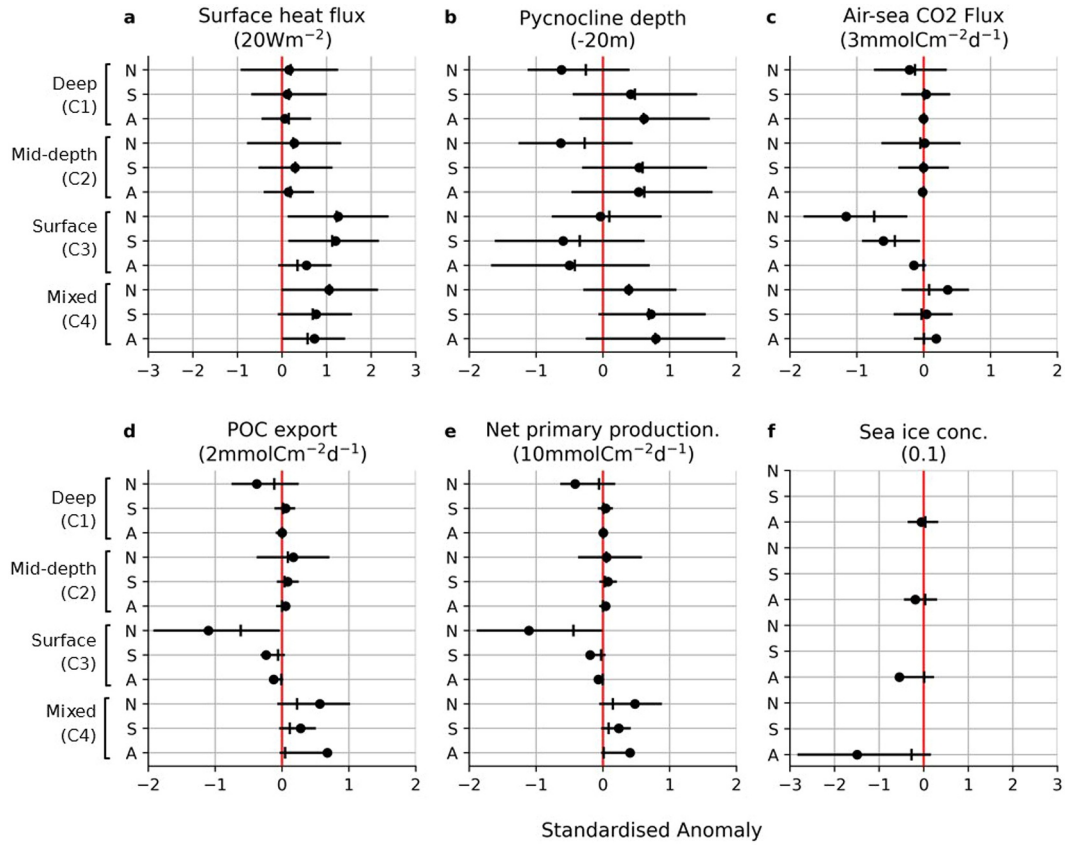


Figure 4. Local physical and biogeochemical anomalies during the detrended CCX. Mean (point), median (vertical line), and interquartile range (horizontal line) of anomalies in (a) surface heat flux into the ocean, (b) pycnocline depth shoaling, (c) air-sea CO_2 flux into the ocean, (d) particulate organic carbon export at 100 m (e) integrated net primary production in the upper 100 m, and (f) sea ice concentration. The units in parenthesis indicate the representative standard deviation by which each variable anomaly was standardized. The y-axis labels denote the cluster type (Deep, Mid-depth, Surface, Mixed) and the zone (Northern, Subantarctic, Antarctic).

the Supporting Information S1. Almost all clusters occur during a significant change in pycnocline depth (Figure 4b), in agreement with the findings of Wong et al. (2024) and Le Grix et al. (2025). Deep and Mid-depth CCX in the Antarctic and Subantarctic zones tend to be associated with an anomalous shoaling of the pycnocline depth (Figure 4b), indicating that they are dynamically driven by the upwelling of warmer and more acidic waters. These subsurface events tend to be decoupled from surface processes, as evidenced by weak changes in surface heat and CO_2 fluxes, sea ice concentration and biological production (Figures 4a and 4c–4f).

CCX clusters with surface MHW expressions (Surface and Mixed clusters) are associated with anomalously high surface heat fluxes (Figure 4a), but differ in the sign of their pycnocline shifts (Figure 4b). The pycnocline deepens during surface CCX in the Subantarctic and Antarctic zones, suggesting that the water column is destabilized during such events. Surface CCX in the Northern zone exhibit a distinct biogeochemical signal, where NPP and POC export are reduced, corresponding to a lower uptake of CO_2 from the atmosphere (Figures 4c–4e). With the Mixed CCX, this effect is reversed, where a shoaling of the pycnocline co-occurs with an increased NPP and POC export. In the Antarctic zone, this also coincides with an anomalously low sea ice concentration (Figure 4f).

3.4. Drivers of MHW During CCX

Next, we investigate the processes driving MHW within each CCX by analyzing local temperature tendencies during the build-up and onset phases of MHW, that is, from the day temperature exceeds the 68th percentile until the day of maximum MHW intensity. We consider both the fractional contribution of each term (Figure 5) and its anomaly relative to the daily climatology (Figure 6). A clear latitudinal pattern emerges in all three zones. In the

19449224, 2026, 10, Downloaded from https://agupubs.onlinelibrary.wiley.com/doi/10.1029/2026GB009430 by Catherine Becker - University Of Southampton , Wiley Online Library on [11/11/2026]. See the Terms and Conditions (https://onlinelibrary.wiley.com/terms-and-conditions) on Wiley Online Library for rules of use; OA articles are governed by the applicable Creative Commons License

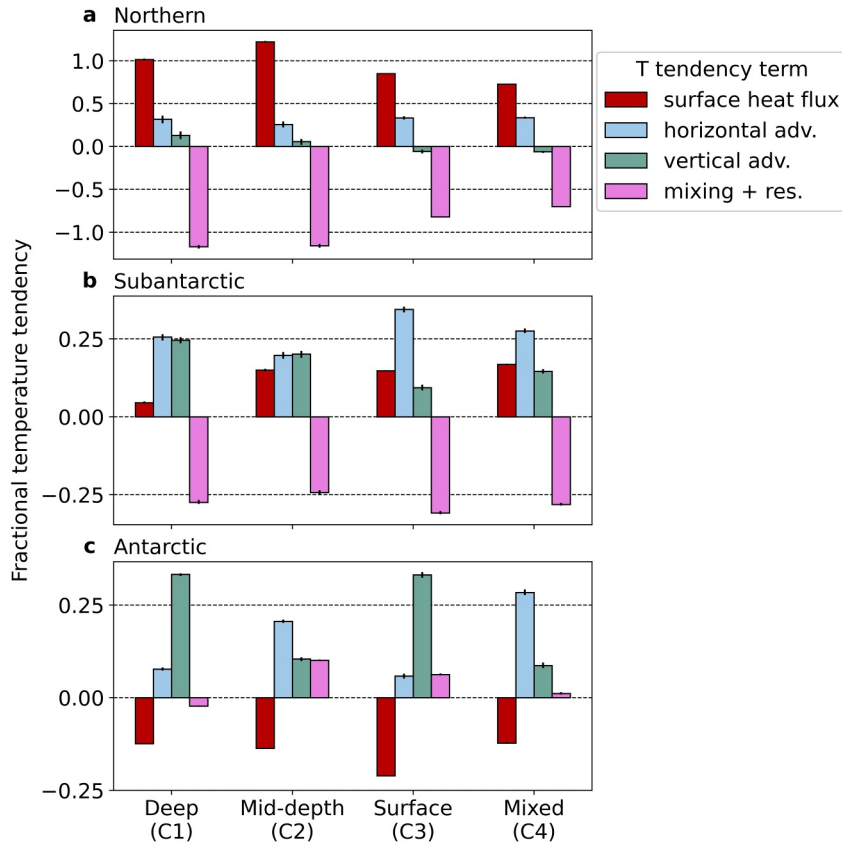


Figure 5. Mean daily temperature tendency terms in MHW grid cells during the build-up and onset of CCX (as a fraction of daily tendency) for the four clusters in the (a) Northern, (b) Subantarctic, and (c) Antarctic zones. The terms shown are surface heat flux (red), horizontal advective flux (light blue), vertical advective flux (green), and a residual term including mixing, diffusion, and convection (pink). Error bars depict the bootstrapped interquartile range (25th–75th percentile).

Northern zone, MHW are driven primarily by surface heat fluxes (Figure 5a), while in the Antarctic zone they are caused by advective heat fluxes and mixing (Figure 5c). The Subantarctic zone exhibits an intermediate regime, with surface and advective heat fluxes contributing substantially to the development of MHW (Figure 5b).

In all clusters in the Antarctic and Subantarctic zones, strong advective heat fluxes, most of which are also anomalously positive, drive the increase in T (Figures 5b and 5c, Figures 6b and 6c). This is consistent with our initial identification of deep and warm waters upwelling as the driver of MHW. The tendency anomalies of Deep CCX (C1) indicate that enhanced vertical advection is the dominant driver of MHW development during CCX (Figure 6c). Positive anomalies in the surface heat flux term further indicate a reduction in surface heat loss during CCX (~7%, Figure 6c), allowing anomalous heat to accumulate. These strong vertical advective heat fluxes transport heat from deeper waters, which are warmer than surface waters in the Antarctic zone (Figure S2 in Supporting Information S1). Although this heat is partially ventilated through a net surface heat loss (Figure 5c), the reduced ventilation during C1 intensifies deep MHW. These warm waters are subsequently transported northward (Bennetts et al., 2024), driving Mid-depth (C2) MHW by horizontal advection of heat (Figures 5c and 6c). Surface CCX (C3) in the Antarctic zone are likewise dominated by vertical advective heat fluxes that are partly compensated by heat loss to the atmosphere (Figure 5c). In contrast to C1 and C2, the deepening of the pycnocline during C3 suggests enhanced vertical exchange, allowing relatively warm subsurface waters to be entrained into the mixed layer.

In the Northern and Subantarctic zones, CCX with surface MHW (C3, C4) are driven primarily by a combination of surface and advective heat fluxes (Figures 5a and 5b). However, anomalies in local surface heat fluxes are relatively weak, contributing 5%−12% to the daily temperature trend (Figures 6a and 6b). In contrast, more than 30% of the temperature tendency is associated with anomalous horizontal advective heat fluxes. In these regions,

19449224, 2026, 10, Downloaded from https://agupubs.onlinelibrary.wiley.com/doi/10.1029/2026GB009430 by Catherine Becker - University Of Southampton , Wiley Online Library on [11/11/2026]. See the Terms and Conditions (https://onlinelibrary.wiley.com/terms-and-conditions) on Wiley Online Library for rules of use; OA articles are governed by the applicable Creative Commons License

19449224, 2026, 10, Downloaded from https://agupubs.onlinelibrary.wiley.com/doi/10.1029/2026GB009430 by Catherine Becker - University Of Southampton , Wiley Online Library on [11/11/2026]. See the Terms and Conditions (https://onlinelibrary.wiley.com/terms-and-conditions) on Wiley Online Library for rules of use; OA articles are governed by the applicable Creative Commons License

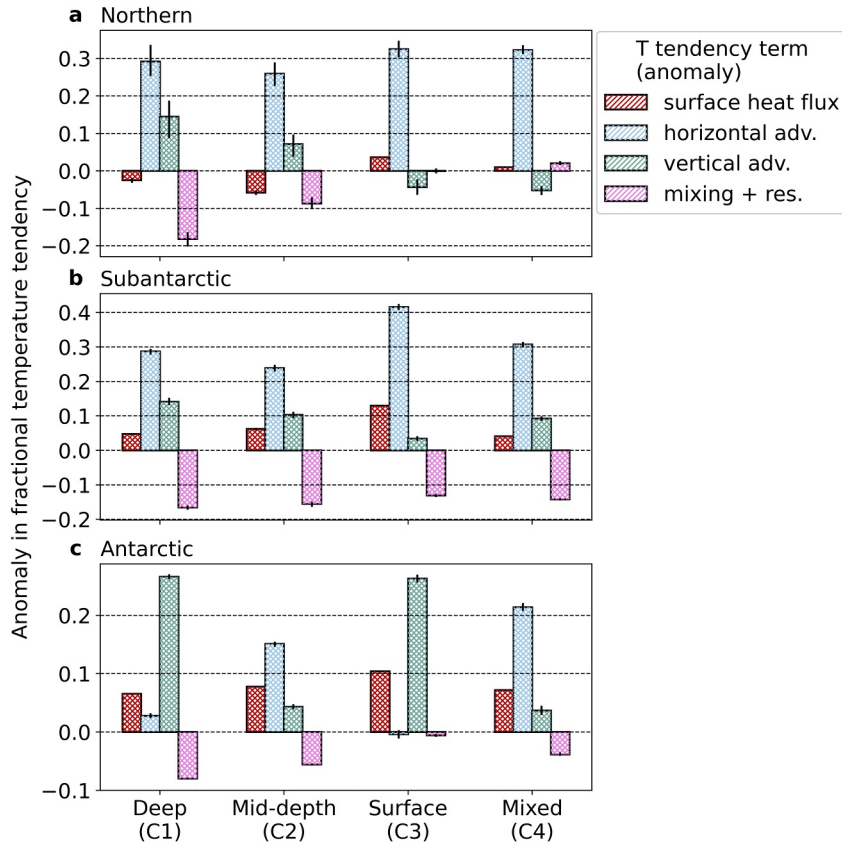


Figure 6. Mean anomalies of fractional daily temperature tendency terms in MHW grid cells during the build-up and onset of CCX for the four clusters in the (a) Northern, (b) Subantarctic, and (c) Antarctic zones. The terms shown are surface heat flux (red), horizontal advective flux (light blue), vertical advective flux (green), and a residual term including mixing, diffusion, and convection (pink). Error bars depict the bootstrapped interquartile range (25th–75th percentile).

MHW may be influenced by meridional shifts of the Antarctic Circumpolar Current, which can transport warmer waters southward and closer to the surface (Figure S2 in Supporting Information S1; Gille, 2013). Thus, although surface heat fluxes drive the baseline warming, the anomalous temperature tendencies during CCX events in the Northern and Subantarctic zones are dominated by horizontal advection.

3.5. Drivers of OAX During CCX

OAX during CCX are caused mainly by a combination of anomalously high T and sDIC, both increasing $[H^+]$ during the onset (Figure 7). Exceptions are found in the Subantarctic (Figure 7b) and in Mixed CCX in the Antarctic (Figure 7c), where anomalies in sAlk tend to be more important than anomalies in sDIC. However, these CCX occur relatively less frequently compared to events of other clusters in other zones (Figure 2c).

In all clusters, increased T accounts for 25%–100% of the anomalous $[H^+]$, as a consequence of the thermodynamic response of the carbonate system in seawater to increasing temperature under isochemical conditions (Sarmiento & Gruber, 2006). For clusters C1 through C3, anomalously high T are expected from MHW co-occurring at the same depths as OAX, underscoring the role of T in driving OAX. For the Mixed cluster (C4), MHW occur at different depths compared to OAX, yet the contribution of T to the $[H^+]$ anomaly is still positive. This indicates that T is elevated throughout the water column, but extreme only in a fraction of the water column.

sDIC anomalies are the dominant contribution to $[H^+]$ anomalies for most clusters in the Antarctic and Northern zone. Given the importance of the sDIC anomalies that underlie OAX, we next look at the physical and biological drivers that affect the carbon balance (Figures 8 and 9) during the build-up and onset of OAX. In most clusters in the Antarctic and Subantarctic zones, the increase in sDIC during OAX in CCX is dominated by contributions from advection and mixing (Figures 8b and 8c). These fluxes are also strongly anomalous during CCX

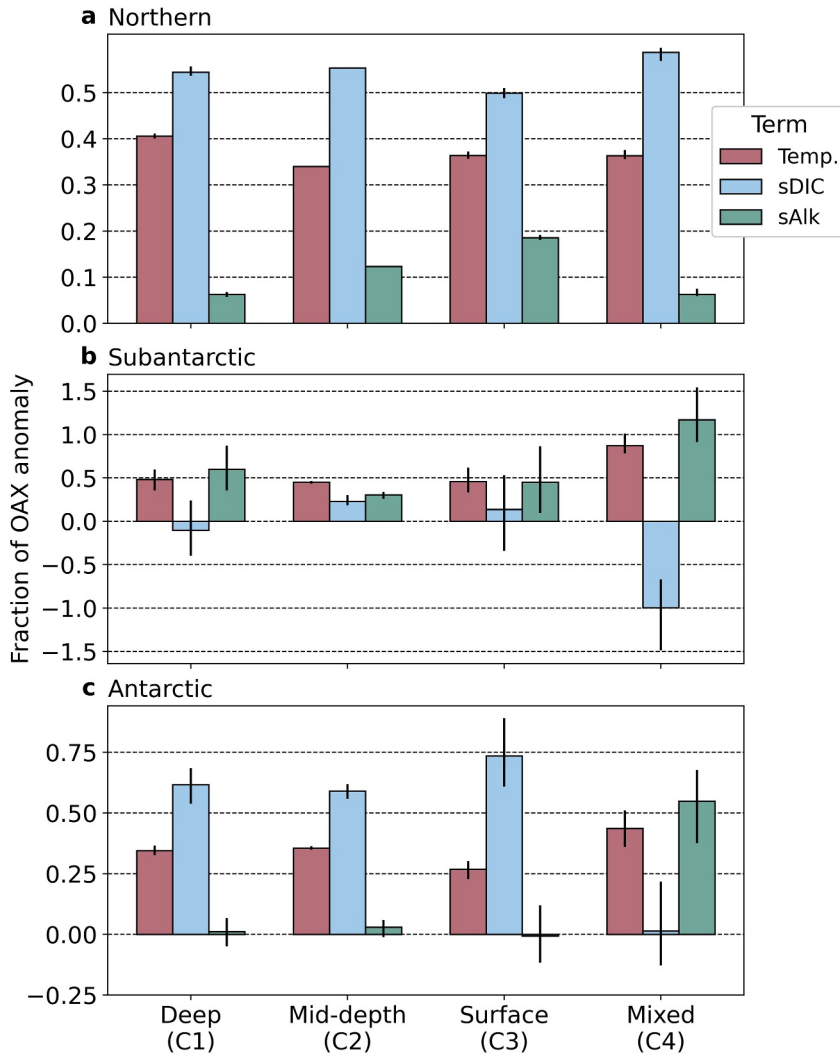


Figure 7. Contribution to the $[H^+]$ anomalies in OAX grid cells from positive anomalies in T and DIC, and negative anomalies in Alk (positive contribution) for the four clusters in the (a) Northern, (b) Subantarctic, and (c) Antarctic zones during the onset of OAX of CCX events. Note the different y-scales for the different panels. Error bars show the bootstrapped interquartile range (25th–75th percentile).

(Figures 9b and 9c). This is consistent with our previous interpretation that many deep and mid-depth CCX are caused by the upwelling of warm and high DIC waters, which bring high $[H^+]$ to the surface (Figures S3-S4 in Supporting Information S1).

In contrast, Surface CCX (C3) with surface OAX tend to be more biologically driven, particularly in the Northern and Subantarctic zones (Figures 8a and 8b). DIC anomalies can be partially explained by the locally reduced NPP. Although the DIC tendency from NPP is always negative (since biological production reduces DIC), their anomalies are positive (Figures 9a and 9b), indicating decreased net DIC consumption when NPP is anomalously low.

In Mixed CCX (C4) with subsurface OAX, local positive sDIC tendencies are driven by increased remineralization of POC (Figures 8 and 9). This effect is seen across all zones and the most strongly in the Northern zone. This is likely a result of the increased biological production in the upper layer described previously (Figures 4d and 4e).

Alkalinity (sAlk) also plays a relatively larger role in driving Mixed CCX in the Antarctic and Subantarctic zones (Figures 7b and 7c). These may be facilitated by an along-isopycnal upwelling of deep waters with lower sAlk

19449224, 2026, 10, Downloaded from https://agupubs.onlinelibrary.wiley.com/doi/10.1029/2026GB009430 by Catherine Becker - University Of Southampton , Wiley Online Library on [11/11/2026]. See the Terms and Conditions (https://onlinelibrary.wiley.com/terms-and-conditions) on Wiley Online Library for rules of use; OA articles are governed by the applicable Creative Commons License

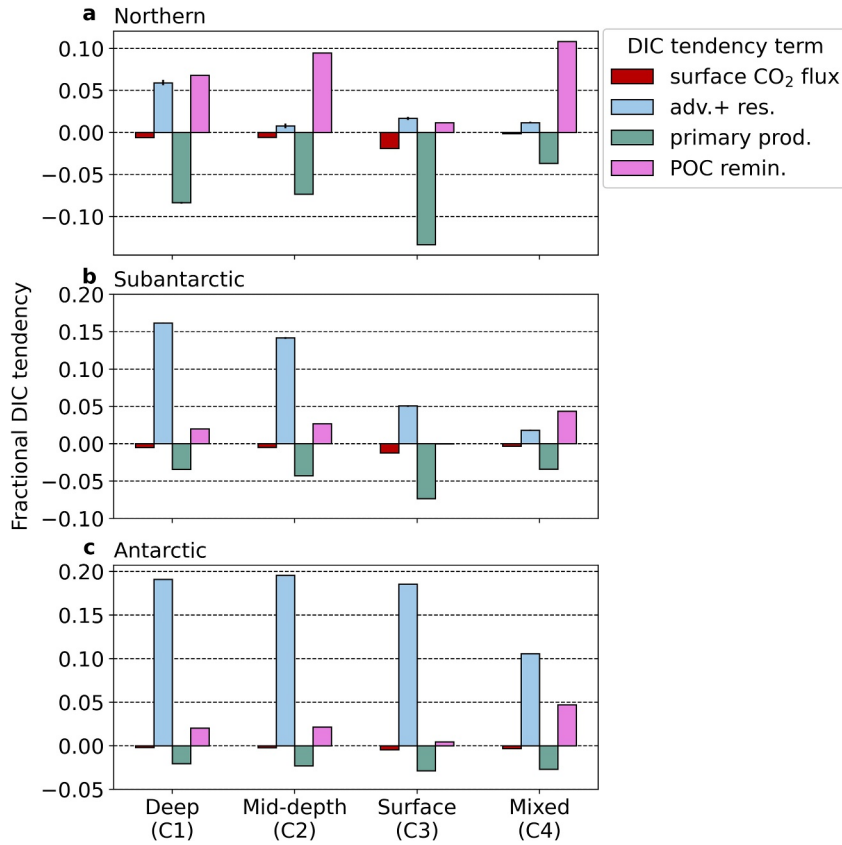


Figure 8. Mean daily DIC tendency terms in OAX grid cells during the build-up and onset of CCX (as a fraction of daily tendency) for the four clusters in the (a) Northern, (b) Subantarctic, and (c) Antarctic zones. The terms shown are surface CO_2 flux (red), advective flux with other dynamic contributions (light blue), negative primary production (green), and particulate organic carbon remineralization (pink). A negative value in "primary prod." indicates a drawdown of DIC due to primary production. Error bars show the bootstrapped interquartile range (25th–75th percentile).

(Figure S5 in Supporting Information S1), coincident with a shoaling of the pycnocline (Figure 4b). However, sAlk tendencies are not analyzed in this study since these events represent a small fraction of CCX in the Southern Ocean.

3.6. Synthesis of Drivers

By focusing on the most prevalent clusters in each zone, we use the above analyses together with the environmental setting to create a synthetic perspective on the drivers underlying the onset of these selected CCX (Figures 2–9). The properties of these selected clusters are summarized in Figure 10. We also report the prevalence of CCX (analyzed in terms of area fraction) in relation to ENSO and SAM (Figure 10e; Table S1 in Supporting Information S1).

3.6.1. Deep and Mid-Depth CCX in the Antarctic Zone (C1, C2)

Deep (C1) and Mid-depth (C2) CCX are the most prevalent events in the Antarctic zone occurring frequently across all seasons. The increase in temperature and DIC can be attributed to an anomalous upwelling of Upper Circumpolar Deep Water, (Marshall & Speer, 2012; Morrison et al., 2015; Nakayama et al., 2018). This is evident in the anomalous heat and DIC tendencies from advective fluxes, and is supported by a shoaled pycnocline (Figure 4b) and increased northward transport (Figures 3a–3h). The composition of $[H^+]$ anomalies further supports Upper Circumpolar Deep Water as its source. High DIC contributions in the absence of air-sea CO_2 flux and POC export anomalies (Figures 4e and 4f) exclude contributions from atmospheric and biological sources.

19449224, 2026, 10, Downloaded from https://agupubs.onlinelibrary.wiley.com/doi/10.1029/2026GB009430 by Catherine Becker - University Of Southampton , Wiley Online Library on [11/11/2026]. See the Terms and Conditions (https://onlinelibrary.wiley.com/terms-and-conditions) on Wiley Online Library for rules of use; OA articles are governed by the applicable Creative Commons License

19449224, 2026, 10, Downloaded from https://agupubs.onlinelibrary.wiley.com/doi/10.1029/2026GB009430 by Catherine Becker - University Of Southampton , Wiley Online Library on [11/11/2026]. See the Terms and Conditions (https://onlinelibrary.wiley.com/terms-and-conditions) on Wiley Online Library for rules of use; OA articles are governed by the applicable Creative Commons License

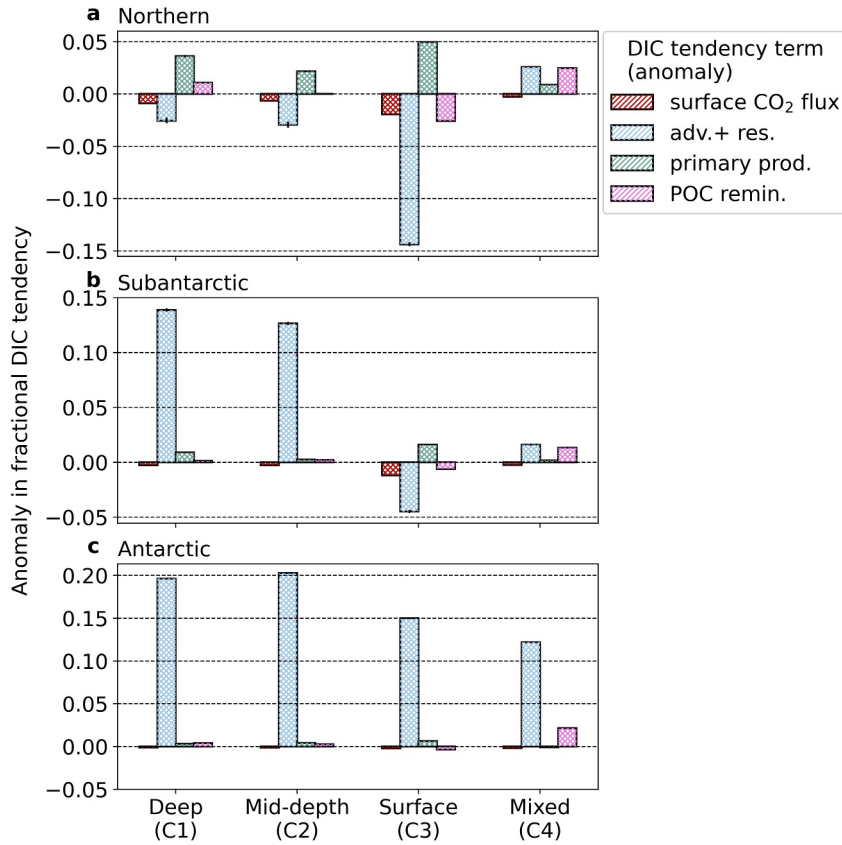


Figure 9. Mean anomalies of fractional daily DIC tendency terms in OAX grid cells during the build-up and onset of CCX for the four clusters in the (a) Northern, (b) Subantarctic, and (c) Antarctic zones. The terms shown are surface CO_2 flux (red), advective flux with other dynamic contributions (light blue), negative primary production (green), and particulate organic carbon remineralization (pink). A positive value in "primary prod." indicates an positive anomalous contribution to DIC from reduced primary production. Error bars show the bootstrapped interquartile range (25th–75th percentile).

Mid-depth CCX differ slightly in their seasonality, with more events occurring in the Austral summer (Figure 2d). They are closer to the continent than Deep CCX (Figure 2b), where the *T* and DIC gradients are steeper in summer (Figures S2 and S4 in Supporting Information S1), and are associated with a typically shallower mixed layer (Figures S6e–S6h in Supporting Information S1) and Winter Water erosion (Bennetts et al., 2024). This leads to MHW and OAX occurring at shallower depths during anomalous upwelling events.

Anomalous upwelling of the Upper Circumpolar Deep Water can be driven by large-scale intensification of westerlies and Ekman divergence that tend to occur during La Niña (LN) and the positive Southern Annular Mode (pSAM) due to low sea level pressure anomalies (Bishop et al., 2016; Hall & Visbeck, 2002; Hogg et al., 2017; Liu et al., 2021; J. Wang et al., 2023). In the hindcast, we find moderate to strong increases in Deep and Mid-depth CCX area during pSAM and LN + pSAM modes, particularly in the Antarctic Pacific sector (Figure 10e). Upper Circumpolar Deep Water as a driving mechanism for subsurface CCX has also been previously identified by Wong et al. (2024) using a lower resolution global ocean model.

3.6.2. Surface CCX in all Zones (C3)

Surface CCX (C3) have distinctly different formation processes in the three zones of the Southern Ocean. In the Antarctic zone during the ice formation season, Surface CCX are driven by the combined effects of advective heat and DIC supply. Despite net surface cooling, positive anomalies in surface heat flux (Figure 4a) indicate a reduction in heat loss relative to climatology. These events are concentrated along the Antarctic coastal margin, where recurring coastal and open-ocean polynyas promote strong ocean–atmosphere coupling during winter sea ice production (Arrigo & van Dijken, 2003; Cheon & Gordon, 2019). An anomalously low sea ice concentration can increase surface momentum transfer, overturning the water column during a period of deep mixed layers and

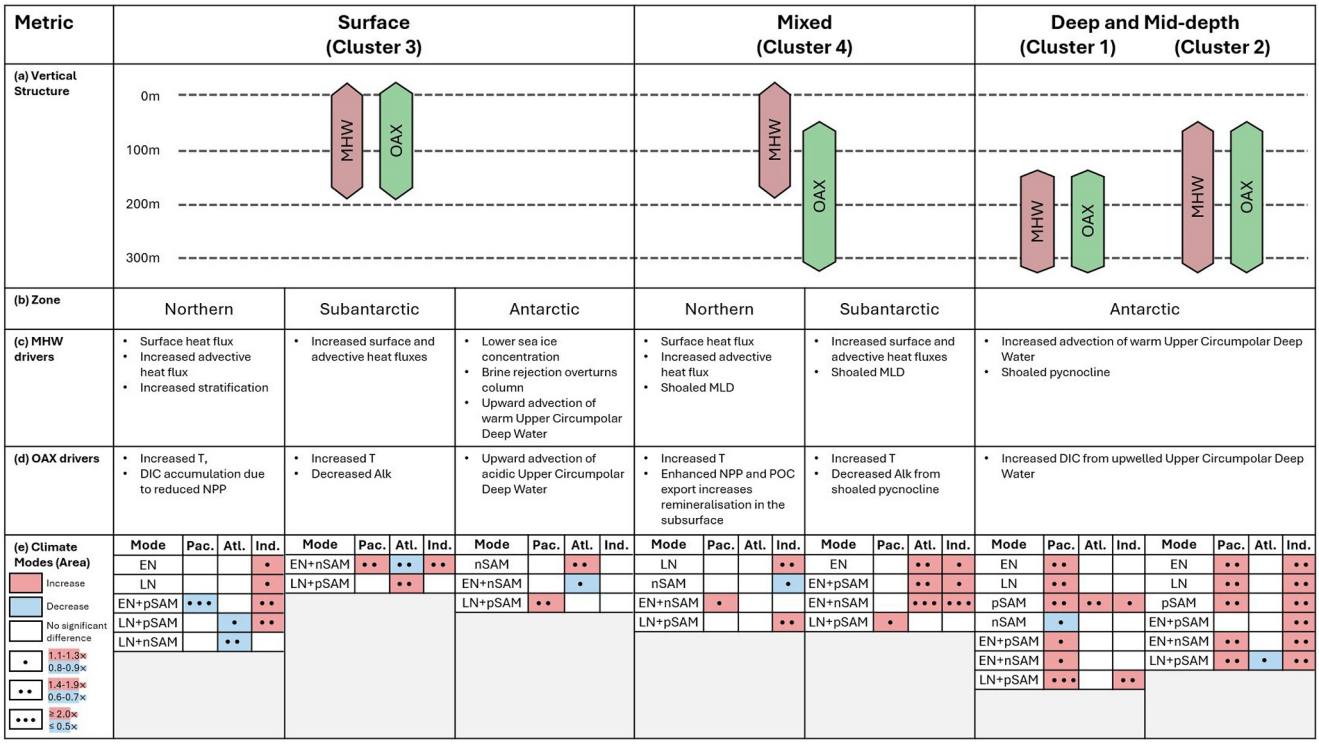


Figure 10. Summary figure describing the properties of the dominant CCX clusters. (a) The vertical structure of MHW and OAX, (b) the zone in which each type of CCX event occurs, (c) identified drivers of MHW, (d) identified drivers of OAX, and (e) CCX area fraction during combinations of El Niño, La Niña, and (positive and negative) SAM with respect to a neutral mode, separated into the Pacific, Atlantic, and Indian sectors, where only significant values (p-value< 0.1) are shaded. Red and blue shading indicate increases and decreases in CCX area, respectively, with the number of dots indicating the magnitude of change.

enabling the vertical entrainment of relatively warm, high-DIC subsurface waters (Ackley et al., 1996; Evans et al., 2018; Morrison et al., 2020). This subsurface ventilation allows surface MHW and OAX to develop during periods of sea-ice formation despite an overall cooling atmospheric forcing (Figure 5c). A moderate increase in Surface CCX is found in the Antarctic Pacific sector during LN + pSAM and the Antarctic Atlantic sector during the negative Southern Annular Mode (nSAM) (Figure 10e).

In the Subantarctic zone, Surface MHW are driven primarily by surface and advective heat fluxes (Figures 5b and 6b), thereby driving OAX by increasing $[H^+]$. OAX is also equally driven by negative sAlk anomalies (Figure 7b), which further reduce buffering and amplify the $[H^+]$ response to warming. At the same time, deepened mixed layers (Figure 4b) driven by wind forcing and buoyancy loss enhance the persistence of surface warm anomalies. Surface CCX area is moderately increased during the in-phase modes of LN + pSAM (Atlantic sector) and the combined El Niño (EN) and nSAM modes (Pacific and Indian Sector), and moderately decreased during EN + nSAM (Atlantic sector), which correspond, respectively, to positive and negative sea surface temperature anomalies found by J. Wang et al. (2023).

In the Northern zone, Surface CCX is associated with distinctly different properties and drivers compared to the other zones. MHW and OAX occur together near the surface with increased occurrence in summer rather than in winter (Figure 2d). Surface heat flux is increased, driving MHW in the upper column and contributing to a thermodynamic increase in $[H^+]$. In the regions where these CCX occur, nutrient limitations in the surface layer are exacerbated, causing NPP and POC export to be significantly reduced (Figures 4d and 4e), increasing the contribution of DIC to $[H^+]$ anomalies. The saturation of DIC on the surface then leads to a net outgassing of CO_2 into the atmosphere (Figure 4c). These Surface CCX in the Northern zone are reflective of surface compounded MHW and OAX found in previous studies (Burger et al., 2022; Wong et al., 2025). The Northern Indian sector sees moderate increases in Surface CCX area during EN + pSAM and LN + pSAM, while the Northern Pacific sector sees strong decreases during EN + pSAM (Figure 10e).

19449224, 2026, 10, Downloaded from https://agupubs.onlinelibrary.wiley.com/doi/10.1029/2026GB009430 by Catherine Becker - University Of Southampton , Wiley Online Library on [11/11/2026]. See the Terms and Conditions (https://onlinelibrary.wiley.com/terms-and-conditions) on Wiley Online Library for rules of use; OA articles are governed by the applicable Creative Commons License

19449224, 2026, 10, Downloaded from https://agupubs.onlinelibrary.wiley.com/doi/10.1029/2026GB009430 by Catherine Becker - University Of Southampton , Wiley Online Library on [11/11/2026]. See the Terms and Conditions (https://onlinelibrary.wiley.com/terms-and-conditions) on Wiley Online Library for rules of use; OA articles are governed by the applicable Creative Commons License

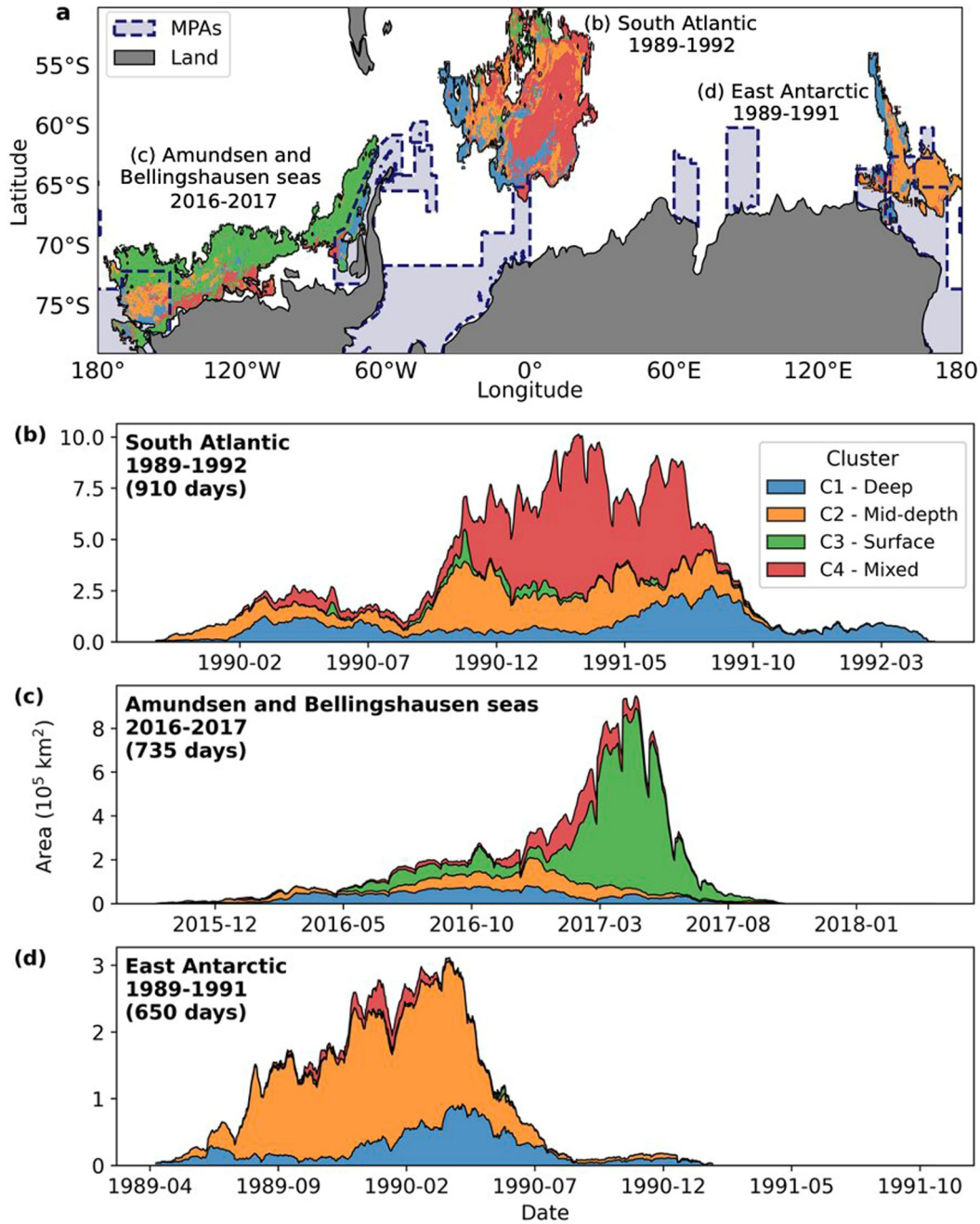


Figure 11. Analyses of selected CCX events. An event is defined by connecting extreme grid cells in space and time. (a)Map showing the maximum spatial extent of the three selected events with the colors representing the mode cluster in each grid cell throughout the course of the event. (b) Timeseries of the stacked cluster area constituting the selected event in the South Atlantic (1989–1992), (c) As (b), but for the Amundsen and Bellingshausen seas event (2016–2017). (d) as (b), but for the East Antarctic event (1989–1991). The time axes has been scaled to the same number of days in plots (b–d).

3.6.3. Mixed CCX in the Subantarctic and Northern Zones (C4)

Mixed CCX are characterized by a surface expression of MHW and subsurface OAX, and are the most prevalent CCX in the Northern and Subantarctic zones. Surface MHW are driven primarily by surface and advective heat fluxes. Heat may be gained cumulatively at the surface, especially in the northern extensions of the Antarctic Circumpolar Current, and transported south along its path (Fernández-Barba et al., 2024). The surface MHW stratifies the water column, leading to a shoaled mixed layer and pycnocline (Figure 4b). Primary production is

19449224, 2026, 10, Downloaded from https://agupubs.onlinelibrary.wiley.com/doi/10.1029/2026GB009430 by Catherine Becker - University Of Southampton , Wiley Online Library on [11/11/2026]. See the Terms and Conditions (https://onlinelibrary.wiley.com/terms-and-conditions) on Wiley Online Library for rules of use; OA articles are governed by the applicable Creative Commons License

stimulated within the shoaled mixed layer, likely due to higher light use efficiency, resulting in increased export of POC and CO_2 uptake from the atmosphere (Figures 4c–4e). Increased POC remineralization and subsequent vertical mixing then drive OAX in the subsurface. We find moderate increases in Mixed CCX area in the Northern Indian sector during LN and LN + pSAM (Figure 10e).

In the Subantarctic zone, subsurface OAX are primarily driven by higher T and lower Alk, with negative anomalies in DIC. Despite anomalously low DIC during OAX, higher temperatures increase $[H^+]$, and this response is further amplified by negative Alk anomalies that reduce buffering capacity. Stratification limits vertical exchange, allowing these temperature and alkalinity driven $[H^+]$ anomalies to persist below the mixed layer. As a result, subsurface OAX can co-occur with surface MHW even when the DIC anomalies are negative. Mixed CCX area increases moderately to strongly in the Indian and Atlantic sectors during EN, EN + nSAM, and EN + pSAM (Figure 10e).

3.7. Case Studies of Large and Long CCX in the Southern Ocean

Three cases of spatially extensive and temporally prolonged CCX events reported by Wong et al. (2025) have been selected and are shown in Figure 11. These cases represent grid-cell CCX events that are connected laterally and in time, enabling us to follow the spatiotemporal evolution of their vertical structures using the clusters defined above. Using the drivers attributed to these clusters in the previous sections, our aim is to construct a storyline following the onset, persistence, and decline of these events.

A common characteristic among the three events in the Subantarctic and Antarctic zones (Figures 11b–11d) is the persistent presence of Deep and Mid-depth CCX (C1, C2). Attributed to an anomalous presence of Upper Circumpolar Deep Water, they created a sustained CCX that persisted for multiple months, in particular over Austral summer when Mid-depth CCX have a tendency to occur. These three events also occurred during the "high" periods of CCX identified in Figure 3b, where the baseline state of the Southern Ocean is characterized by a shallower pycnocline depth, a result of wind-driven anomalous Ekman divergence. The event in the East Antarctic (Figure 11d) is dominated by these two clusters, beginning in April 1989 near the East Antarctic coast. As Mid-depth CCX quickly reaches a maximum area and plateaus, Deep CCX begins to increase in area northward. Deep CCX occur farther from the coast and deeper in the column, corresponding to deeper pycnoclines at 55°S (Figures S6a–S6d in Supporting Information S1). The event tapers quickly toward July as sea ice formation occurs, destabilizing the water column and deepening the pycnocline.

In Figures 11b and 11c, we find Surface and Mixed CCX (C3, C4) occurring in shorter durations but covering 3–4 times the affected area compared to the Deep and Mid-depth events. In the Amundsen and Bellingshausen seas (Figure 11c), mostly subsurface CCX occur in the area close to the coast throughout 2016. Then in 2017, after a period of anomalously low sea ice (Stuecker et al., 2017; Z. Wang et al., 2019), large areas of Surface CCX developed within the sea ice zone and close to the edge of the marginal ice zone in the Bellingshausen Sea. The total CCX area reached a peak of almost 900,000 km^2. During the period of sea ice formation, the anomalously low sea ice facilitated the increase in surface momentum flux, entraining Upper Circumpolar Deep Water to the surface. The event declines quickly after May, ending in September, when the extent of sea ice is typically at its maximum.

In the South Atlantic (Figure 11b), the area of Mixed CCX (C4) increases in the summer of 1990, until the total CCX area covered almost 1,000,000 km^2 in March 1991. MHW at the surface is driven by anomalous surface and horizontal advective heat fluxes. The mixed layer and the pycnocline shoaled, leading to OAX induced by higher temperatures and lower sAlk. This is further exacerbated by anomalously low sea ice in 1991 (Cavalieri & Parkinson, 2008; Zwally et al., 2002) during the period of sea ice formation.

4. Discussion

4.1. CCX in the Southern Ocean Are Dynamically Driven

The dominant clusters in each zone and their characteristics are summarized in Figure 10. We find that many of these events are primarily or partially facilitated by dynamic shifts in gradients and advective fluxes. A primary source of heat and acidity in the Southern Ocean is the upwelling of Upper Circumpolar Deep Water, which enters the Southern Ocean as deep water from other basins (Bennetts et al., 2024; Evans et al., 2018) and can increase during an intensification of westerlies (Hogg et al., 2017). Our study shows that this mechanism drives Deep and

19449224, 2026, 10, Downloaded from https://agupubs.onlinelibrary.wiley.com/doi/10.1029/2026GB009430 by Catherine Becker - University Of Southampton , Wiley Online Library on [11/11/2026]. See the Terms and Conditions (https://onlinelibrary.wiley.com/terms-and-conditions) on Wiley Online Library for rules of use; OA articles are governed by the applicable Creative Commons License

Mid-depth CCX events in the Antarctic zone, which occurred more frequently during 1985–1994 and 2015–2019 (Figures 3a and 3b), coinciding with periods of stronger northward surface transport (Figure 3f). The increase in the occurrence of these CCX during pSAM and LN + pSAM modes is notable (Figure 10e), as J. Wang et al. (2023) showed that they are correlated with lower pressure over the Antarctic continent and stronger westerlies south of 60°S. Furthermore, the vertical extent of these events is modulated by surface stratification. The presence of fresh, light Antarctic Surface Waters near the surface during summer can inhibit the upwelling and ventilation of the Upper Circumpolar Deep Water at the surface (Evans et al., 2018), likely restricting CCX to mid-depths. In winter, the upper water column is destabilized by surface cooling and brine rejection (Bennetts et al., 2024), allowing Upper Circumpolar Deep Water to rise to the surface and likely contributing to Surface CCX in the Antarctic zone. The convective overturning during winter induces Surface CCX with anomalously deep pycnocline and mixed-layer depths. Thus, the vertical distribution of CCX in the Antarctic zone can be understood primarily as a modulation of deep water upwelling and convective mixing, which regulate the extent to which its heat and DIC anomalies reach the upper ocean.

CCX events with surface MHWs in the Northern and Subantarctic zones show a greater contribution from advective heat fluxes, consistent with previous studies identifying oceanic advection as an important driver of MHWs (Holbrook et al., 2019; Sala et al., 2025; Zhang et al., 2023). In particular, the presence of strong currents can enhance the redistribution of heat and contribute to local MHW development. Our results show that, although events in the Northern zone remain predominantly driven by surface heat fluxes, anomalous advective heat fluxes during CCX events account for up to 30% of the daily temperature tendency (Figures 5 and 6). The spatial progression of these events along the Antarctic Circumpolar Current further suggests that advective heat transport contributes to their propagation (Figure 2b). This reveals an important characteristic of MHWs in the Southern Ocean, where extreme surface warming can be maintained or enhanced not only by surface forcing but also by ocean dynamics, particularly in regions influenced by strong currents.

4.2. Surface MHW Drive OAX by Modulating Biological Production

Previous studies have identified surface MHWs as a potential driver of increased NPP in the Southern Ocean (Fernández-Barba et al., 2024; Montie et al., 2020). This has been attributed to the concentration of light and nutrients within a shoaled mixed layer (Pinkerton et al., 2021), which are key factors limiting production at high latitudes. Our results show a similar response during Mixed CCX events in the Northern and Subantarctic zones. During these events, the pycnocline is anomalously shoaled (Figure 4b). They occur in regions characterized by strong currents (Figure 2b), where diapycnal mixing can supply nutrients to the upper ocean. Consistent with these conditions, we find enhanced NPP in the upper 100 m, accompanied by increased POC export to the subsurface (Figures 4d and 4e). This is accompanied by an increase in DIC production from remineralization (Figures 8 and 9), which contributes to subsurface OAX during these events.

On the other hand, we find an opposite effect in Surface CCX in the Northern and Subantarctic zones, which are located in regions with lower nutrient supply and typically lower biological production and export (Figure 2b; Figure S7 in Supporting Information S1). Here, increased stratification from surface MHW inhibits upwelling, reducing primary production, and inducing OAX on the surface with an abnormal retention of DIC (Figures 4, 7–9).

4.3. Anomalies in Sea Ice Concentration Drive Decadal Variability in CCX

Our results show a negative correlation between sea ice concentration and the frequency of CCX events in the Antarctic zone, with periods of lower sea ice concentration coinciding with increased CCX occurrence across all clusters (Figure 3). Previous studies have identified several mechanisms through which anomalous sea ice conditions may be associated with enhanced ocean heat and carbon transport into the surface ocean. Stronger westerlies and enhanced deep-water upwelling can contribute to anomalous sea ice retreat (Lee et al., 2017). Conversely, reduced sea ice extent at the northern ice edge can increase surface stress and Ekman divergence, promoting upwelling of warm and carbon-rich Upper Circumpolar Deep Water (Ramadhan et al., 2022). Increased surface momentum stress can also destabilize the upper water column and enhance vertical mixing of subsurface waters into the surface (Pellichero et al., 2017). These processes provide possible physical mechanisms linking the low sea ice conditions to the increased CCX occurrence that we find in the Antarctic zone.

19449224, 2026, 10, Downloaded from https://agupubs.onlinelibrary.wiley.com/doi/10.1029/2026GB009430 by Catherine Becker - University Of Southampton , Wiley Online Library on [11/11/2026]. See the Terms and Conditions (https://onlinelibrary.wiley.com/terms-and-conditions) on Wiley Online Library for rules of use; OA articles are governed by the applicable Creative Commons License

In particular, low sea ice concentrations occur during 1985–1994 and 2015–2019 (Figure 3j), coinciding with periods of high CCX occurrence. This co-occurrence suggests that periods of anomalously low sea ice may favor the simultaneous exposure of Antarctic surface waters to high temperatures and high acidity, producing a potential "triple compound" of high temperature, high acidity, and low sea ice. Such conditions may pose additional risks to sympagic organisms such as copepods and amphipods, which depend on sea ice for recruitment, growth, and overwintering. For example, larval and juvenile Antarctic krill depend on sea ice algae as a food source and on the physical structure of sea ice for protection from predators during winter (Frazer, 1996; Marschall, 1988; Quetin & Ross, 2009).

4.4. ENSO and SAM Drive CCX on Sub-Zonal Scales

Large-scale climate modes such as ENSO and SAM have previously been shown to influence extreme variability in the Southern Ocean (Holbrook et al., 2019), but we found their influence on CCX in the Southern Ocean to be less strong. In our analysis, ENSO, SAM, and their combinations are associated with CCX clusters in a zonally asymmetric manner (Figure 10e). This spatial asymmetry is consistent with the composite analysis of J. Wang et al. (2023), who found zonally asymmetric responses of surface heat fluxes, sea ice concentration, and sea level pressure anomalies to different combinations of the two modes. In particular, they found that the in-phase combination of LN + pSAM was associated with negative sea ice anomalies in the Bellingshausen Sea and Atlantic sector, which corresponds spatially to the occurrence of Surface CCX in the Antarctic zone (C3) in our analysis. Similarly, their association of EN + nSAM with negative sea ice anomalies in the Indian and Pacific sectors is consistent with the occurrence of Mixed CCX (C4) in the Subantarctic zone in our analysis.

In contrast, the out-of-phase combinations EN + pSAM and LN + nSAM show weaker associations with changes in CCX occurrence. The absence of a clear interannual response to the combined effects of ENSO and SAM may partly reflect the relatively short decorrelation timescale of SAM, approximately 10 days, despite its importance as a mode of Southern Ocean variability (Fogt & Marshall, 2020). Nevertheless, the sector-level associations identified here suggest that large-scale climate modes can influence the spatial occurrence of CCX and may help distinguish the vertical structure, duration, and intensity of events associated with different modes of variability.

4.5. Drivers of CCX Inform Predictability and Biological Impact

Beyond explaining the observed variability in CCX, the drivers identified in this study provide a basis for anticipating when and where different types of CCX may occur and, consequently, their potential biological impacts. In particular, associations between CCX and readily observable environmental conditions such as sea surface temperature, wind stress, and sea ice cover could provide indicators of the probable seasonality, vertical structure, intensity, and duration of events. For example, the association between La Ni na–positive SAM conditions and Surface CCX in the Antarctic Pacific sector suggests that periods of anomalous atmospheric and oceanic forcing could coincide with conditions that are particularly challenging for sea ice-associated organisms. Such events may reduce suitable sea ice habitat for grazers such as the Antarctic copepod (*Calanus propinquus*) and krill (*Euphausia superba*) (Schmidt et al., 2014), while simultaneously exposing them to anomalously warm and acidic waters. This may be particularly consequential during winter, when newly hatched krill larvae are vulnerable to anomalous temperature and acidity and survival through their first winter is an important determinant of subsequent recruitment success (Daly, 2004; Kawaguchi et al., 2011, 2013; Lowe et al., 2012).

Mixed CCX (C4) in the Northern zone extend across a large vertical range, with elevated temperatures in the upper water column and elevated $[H^+]$ below 100 m, potentially reducing the vertical habitable space available to vulnerable organisms (Figures 2a and 2g). Vertically migrating zooplankton may benefit from enhanced food availability during such events, but could also experience increased metabolic demands under warmer and more acidic conditions. Although this study does not quantify the biological impacts of CCX directly, it indicates potential risks to marine organisms and habitats, particularly if the frequency or intensity of such events increases in the future.

5. Caveats and Limitations

This study is limited in that it has only attributed the CCX drivers during their onset, but has not identified the mechanisms that underlie their decline. These decline mechanisms may be climatic, seasonal, or induced by

19449224, 2026, 10, Downloaded from https://agupubs.onlinelibrary.wiley.com/doi/10.1029/2026GB009430 by Catherine Becker - University Of Southampton , Wiley Online Library on [11/11/2026]. See the Terms and Conditions (https://onlinelibrary.wiley.com/terms-and-conditions) on Wiley Online Library for rules of use; OA articles are governed by the applicable Creative Commons License

negative feedbacks to extreme conditions and limit the duration of events in possibly predictable ways. Understanding the conditions that lead to the decline of CCX is also important, since the absence of these decline mechanisms may be seen as a driver of the persistence of extreme events (Burger & Frölicher, 2023; Schlegel et al., 2021; A. Sen Gupta et al., 2020; Spillman et al., 2021). Quantifying the role of decline mechanisms as drivers and terminators of CCX could be a valuable direction for future research.

Another limitation of this study lies in the choice of drivers considered in the analysis. In the attribution of H^+ anomalies (Equation 1), contributions from changes in salinity, silicate, and phosphate were omitted. Similarly, in the decomposition of temperature and DIC tendencies (Equations 2 and 3), several comparatively small terms were aggregated into broader terms. Consequently, the contributions of these omitted or aggregated processes are not explicitly resolved and may contribute to the residual variability in the dominant terms analyzed during CCX.

Due to data limitation, the sea ice freshwater forcing flux used to drive this model was quite simplistically prescribed in the form of a climatology imposed on a linear trend. Thus, apart from the linear trend, there is no interannual variation in the sea ice freshwater fluxes. During the melting and freezing seasons, anomalous freshwater fluxes can modulate buoyancy, which we have shown to be a driver of CCX in the Southern Ocean. Therefore, a more accurate observational data set on melting and freezing fluxes could potentially identify these fluxes as drivers of CCX on an interannual timescale. Due to this limitation in model forcing, we have largely excluded the attribution of CCX to sea ice freshwater fluxes in this study.

Finally, the 1/4° spatial resolution of the ROMS model is insufficient to resolve mesoscale eddies and other mesoscale features in the high latitude Southern Ocean. A model resolution of at least 1/12° is needed to resolve such processes in the Antarctic Circumpolar Current (Hallberg, 2013). Eddies in the Southern Ocean potentially play an important role as drivers of CCX due to their abundance in the energetic Antarctic Circumpolar Current (Frenger et al., 2015; Thompson, 2008), their ability to laterally transport heat and carbon (Bian et al., 2023; Moreau et al., 2017; Olbers et al., 2004) and upwell or uptake carbon (Jones et al., 2017; Keppler et al., 2024; Taylor et al., 2018).

6. Conclusion

Column-compound MHW and OAX are widespread across the Southern Ocean, spanning different depths of the upper water column. We show that Deep (∼200–300 m) and Mid-depth (∼150 m) CCX dominate the Antarctic zone and are driven primarily by anomalous upwelling of warm and DIC-rich subsurface waters. This upwelling is modulated by sea-ice cover and northward transport of surface waters, and occurred more frequently during La Niña conditions and the positive phase of the SAM. In the Northern zone, Surface and Mixed CCX are more prevalent, where surface MHW drive OAX by modulating primary production. In strongly stratified regions, MHW suppress nutrient supply and promote DIC retention and hence OAX in the surface ocean. In contrast, where vertical mixing and nutrient supply is strong, MHW stimulate production and POC export, driving OAX in the subsurface through increased remineralization. Overall, our results demonstrate that CCX are governed by shifts in the balance between physical circulation and biological processes. These findings improve our mechanistic understanding of column-compound MHW and OAX in the Southern Ocean and provide a foundation for future studies of their predictability and response to climate change.

Conflict of Interest

The authors declare no conflicts of interest relevant to this study.

Availability Statement

The ROMS-BEC hindcast used in this study is described and evaluated in Wong et al. (2025). All scripts used for data processing, evaluation, and analysis, and the data required for all plots can be found in the following repository (Wong et al., 2026): https://doi.org/10.3929/ethz-c-000802906.

Acknowledgments
The authors thank Dr. Damian Loher and Dr. Mark Hague for their modeling support with the ROMS-BEC hindcast runs. We acknowledge support from the European Union's Horizon 2020 research and innovation program under Grant agreement No. 820989 (COMFORT). The authors also thank the two reviewers for their time and expertise in improving the quality and clarity of this manuscript. Open access publishing facilitated by Eidgenossische Technische Hochschule Zurich, as part of the Wiley - Eidgenossische Technische Hochschule Zurich agreement via the Consortium Of Swiss Academic Libraries.

References

Ackley, S. F., Fritsen, C., Lytle, V., & Sullivan, C. (1996). Freezing driven upwelling in Antarctic sea ice biological systems. In *Proceedings of the NIPR symposium on polar biol* (Vol. 9).

Arrigo, K. R., & van Dijken, G. L. (2003). Phytoplankton dynamics within 37 Antarctic coastal polynya systems. *Journal of Geophysical Research*, *108*(C8). https://doi.org/10.1029/2002JC001739

Bennetts, L. G., Shakespeare, C. J., Vreugdenhil, C. A., Foppert, A., Gayen, B., Meyer, A., et al. (2024). Closing the loops on Southern Ocean dynamics: From the circumpolar current to ice shelves and from bottom mixing to surface waves. *Reviews of Geophysics*, *62*(3), e2022RG000781. https://doi.org/10.1029/2022RG000781

Bian, C., Jing, Z., Wang, H., Wu, L., Chen, Z., Gan, B., & Yang, H. (2023). Oceanic mesoscale eddies as crucial drivers of global marine heatwaves. *Nature Communications*, *14*(1), 2970. https://doi.org/10.1038/s41467-023-38811-z

Bishop, S. P., Gent, P. R., Bryan, F. O., Thompson, A. F., Long, M. C., & Abernathey, R. (2016). Southern Ocean overturning compensation in an eddy-resolving climate simulation. *Journal of Physical Oceanography*, *46*(5), 1575–1592. https://doi.org/10.1175/JPO-D-15-0177.1

Burger, F. A., & Frölicher, T. L. (2023). Drivers of surface ocean acidity extremes in an Earth system model. *Global Biogeochemical Cycles*, *37*(9), e2023GB007785. https://doi.org/10.1029/2023GB007785

Burger, F. A., Terhaar, J., & Frölicher, T. L. (2022). Compound marine heatwaves and ocean acidity extremes. *Nature Communications*, *13*, 1–12. https://doi.org/10.1038/s41467-022-32120-7

Cavalieri, D. J., & Parkinson, C. L. (2008). Antarctic sea ice variability and trends, 1979–2006. *Journal of Geophysical Research*, *113*(C7). https://doi.org/10.1029/2007JC004564

Cheon, W. G., & Gordon, A. L. (2019). Open-ocean polynyas and deep convection in the Southern Ocean. *Scientific Reports*, *9*(1), 6935. https://doi.org/10.1038/s41598-019-43466-2

Constable, A. J., Melbourne-Thomas, J., Muelbert, M. M. C., McCormack, S., Brasier, M., Caccavo, J. A., et al. (2023). Marine ecosystem assessment for the Southern Ocean: Summary for policymakers (Technical Report). https://doi.org/10.5281/zenodo.8359585

Daly, K. L. (2004). Overwintering growth and development of larval *Euphausia superba*: An interannual comparison under varying environmental conditions west of the Antarctic Peninsula. *Deep Sea Research Part II: Topical Studies in Oceanography*, *51*(17), 2139–2168. https://doi.org/10.1016/j.dsr2.2004.07.010

Delille, B., Vancoppenolle, M., Geilfus, N.-X., Tilbrook, B., Lannuzel, D., Schoemann, V., et al. (2014). Southern Ocean CO2 sink: The contribution of the sea ice. *Journal of Geophysical Research: Oceans*, *119*(9), 6340–6355. https://doi.org/10.1002/2014JC009941

Eayrs, C., Li, X., Raphael, M. N., & Holland, D. M. (2021). Rapid decline in Antarctic sea ice in recent years hints at future change. *Nature Geoscience*, *14*(7), 460–464. https://doi.org/10.1038/s41561-021-00768-3

Eisbrenner, E. (2025). Lagrangian attribution of marine heatwave drivers. *Environmental Research Communications*, *7*(11), 111007. https://doi.org/10.1088/2515-7620/ae0f81

Elzahaby, Y., Schaeffer, A., Roughan, M., & Delaux, S. (2021). Oceanic circulation drives the deepest and longest marine heatwaves in the east Australian current system. *Geophysical Research Letters*, *48*(17), e2021GL094785. https://doi.org/10.1029/2021GL094785

Evans, D. G., Zika, J. D., Naveira Garabato, A. C., & Nurser, A. J. (2018). The cold transit of Southern Ocean upwelling. *Geophysical Research Letters*, *45*(24), 13386–13395. https://doi.org/10.1029/2018GL079986

Fernández-Barba, M., Belyaev, O., Huertas, I. E., & Navarro, G. (2024). Marine heatwaves in a shifting Southern Ocean induce dynamical changes in primary production. *Communications Earth & Environment*, *5*(1), 1–15. https://doi.org/10.1038/s43247-024-01553-x

Fogt, R. L., & Marshall, G. J. (2020). The Southern Annular Mode: Variability, trends, and climate impacts across the Southern Hemisphere. *WIREs Climate Change*, *11*(4), e652. https://doi.org/10.1002/wcc.652

Frazer, T. K. (1996). Stable isotope composition (13C and 15N) of larval krill, Euphausia superba, and two of its potential food sources in winter. *Journal of Plankton Research*, *18*(8), 1413–1426. https://doi.org/10.1093/plankt/18.8.1413

Frenger, I., Münnich, M., Gruber, N., & Knutti, R. (2015). Southern Ocean eddy phenomenology. *Journal of Geophysical Research: Oceans*, *120*(11), 7413–7449. https://doi.org/10.1002/2015JC011047

Gille, S. T. (2013). Meridional displacement of the Antarctic circumpolar current. *Philosophical Transactions of the Royal Society A: Mathematical, Physical and Engineering Sciences*, *372*(2019), 20130273. https://doi.org/10.1098/rsta.2013.0273

Godoi, V. A., & Torres Júnior, A. R. (2020). A global analysis of austral summer ocean wave variability during SAM–ENSO phase combinations. *Climate Dynamics*, *54*(9), 3991–4004. https://doi.org/10.1007/s00382-020-05217-2

Gomes, D. G. E., Ruzicka, J. J., Crozier, L. G., Huff, D. D., Brodeur, R. D., & Stewart, J. D. (2024). Marine heatwaves disrupt ecosystem structure and function via altered food webs and energy flux. *Nature Communications*, *15*(1), 1988. https://doi.org/10.1038/s41467-024-46263-2

Gong, D., & Wang, S. (1999). Definition of Antarctic oscillation index. *Geophysical Research Letters*, *26*(4), 459–462. https://doi.org/10.1029/1999GL900003

Gruber, N., Boyd, P. W., Frölicher, T. L., & Vogt, M. (2021). Ocean biogeochemical extremes and compound events. *Nature*, *600*(7889), 395–407. https://doi.org/10.1038/s41586-021-03981-7

Guibourd de Luzinais, V., Gascuel, D., Reygondeau, G., & Cheung, W. W. L. (2024). Large potential impacts of marine heatwaves on ecosystem functioning. *Global Change Biology*, *30*(7), e17437. https://doi.org/10.1111/gcb.17437

Hague, M., Münnich, M., & Gruber, N. (2024). Zonally asymmetric increase in Southern Ocean heat content. *Journal of Climate*, *37*(24), 6585–6604. https://doi.org/10.1175/JCLI-D-23-0623.1

Hall, A., & Visbeck, M. (2002). Synchronous variability in the Southern Hemisphere atmosphere, sea ice, and ocean resulting from the annular mode. *Journal of Climate*, *15*(21), 3043–3057. https://doi.org/10.1175/1520-0442(2002)015<3043:svitsh>2.0.co;2

Hallberg, R. (2013). Using a resolution function to regulate parameterizations of oceanic mesoscale eddy effects. *Ocean Modelling*, *72*, 92–103. https://doi.org/10.1016/j.ocemod.2013.08.007

Haumann, F. A., Gruber, N., Münnich, M., Frenger, I., & Kern, S. (2016). Sea-ice transport driving Southern Ocean salinity and its recent trends. *Nature*, *537*(7618), 89–92. https://doi.org/10.1038/nature19101

Hersbach, H., Bell, B., Berrisford, P., Hirahara, S., Horányi, A., Muñoz-Sabater, J., et al. (2020). The ERA5 global reanalysis. *Quarterly Journal of the Royal Meteorological Society*, *146*(730), 1999–2049. https://doi.org/10.1002/qj.3803

Hobday, A. J., Alexander, L. V., Perkins, S. E., Smale, D. A., Straub, S. C., Oliver, E. C., et al. (2016). A hierarchical approach to defining marine heatwaves. *Progress in Oceanography*, *141*, 227–238. https://doi.org/10.1016/j.pocean.2015.12.014

Hogg, A. M., Spence, P., Saenko, O. A., & Downes, S. M. (2017). The energetics of Southern Ocean upwelling. *Journal of Physical Oceanography*, *47*(1), 135–153. https://doi.org/10.1175/JPO-D-16-0176.1

Holbrook, N. J., Scannell, H. A., Sen Gupta, A., Benthuysen, J. A., Feng, M., Oliver, E. C., et al. (2019). A global assessment of marine heatwaves and their drivers. *Nature Communications*, *10*(1), 1–13. https://doi.org/10.1038/s41467-019-10206-z

Jacox, M. G. (2019). Marine heatwaves in a changing climate. *Nature*, *571*(7766), 485–487. https://doi.org/10.1038/d41586-019-02196-1

Jones, E. M., Fenton, M., Meredith, M. P., Clargo, N. M., Ossebaar, S., Ducklow, H. W., et al. (2017). Ocean acidification and calcium carbonate saturation states in the coastal zone of the West Antarctic Peninsula. *Deep-Sea Research Part II Topical Studies in Oceanography*, *139*, 181–194. https://doi.org/10.1016/j.dsr2.2017.01.007

Kawaguchi, S., Ishida, A., King, R., Raymond, B., Waller, N., Constable, A., et al. (2013). Risk maps for Antarctic krill under projected Southern Ocean acidification. *Nature Climate Change*, *3*(9), 843–847. https://doi.org/10.1038/nclimate1937

19449224, 2026, 10, Downloaded from https://agupubs.onlinelibrary.wiley.com/doi/10.1029/2026GB009430 by Catherine Becker - University Of Southampton , Wiley Online Library on [11/11/2026]. See the Terms and Conditions (https://onlinelibrary.wiley.com/terms-and-conditions) on Wiley Online Library for rules of use; OA articles are governed by the applicable Creative Commons License

Kawaguchi, S., Kurihara, H., King, R., Hale, L., Berli, T., Robinson, J. P., et al. (2011). Will krill fare well under Southern Ocean acidification? *Biology Letters*, *7*(2), 288–291. https://doi.org/10.1098/rsbl.2010.0777

Keppler, L., Eddebbar, Y. A., Gille, S. T., Guisewhite, N., Mazloff, M. R., Tamsitt, V., et al. (2024). Effects of mesoscale eddies on Southern Ocean biogeochemistry. *AGU Advances*, *5*(6), e2024AV001355. https://doi.org/10.1029/2024AV001355

Kohlman, C., Mogen, S., Cohen, J. T., Araujo, J., Beaudin, E., Bonino, G., et al. (2025). Surface and subsurface biogeochemical impacts of the 2019 Northeast Pacific marine heatwave. *Geophysical Research Letters*, *52*(16), e2025GL115230. https://doi.org/10.1029/2025GL115230

Köhn, E. E., Vogt, M., Münnich, M., & Gruber, N. (2024). On the vertical structure and propagation of marine heatwaves in the Eastern Pacific. *Journal of Geophysical Research: Oceans*, *129*(1), e2023JC020063. https://doi.org/10.1029/2023JC020063

Lauvset, S. K., Key, R. M., Olsen, A., van Heuven, S., Velo, A., Lin, X., et al. (2016). A new global interior ocean mapped climatology: The 1° × 1° GLODAP version 2. *Earth System Science Data*, *8*(2), 325–340. https://doi.org/10.5194/essd-8-325-2016

Lee, S.-K., Volkov, D. L., Lopez, H., Cheon, W. G., Gordon, A. L., Liu, Y., & Wanninkhof, R. (2017). Wind-driven ocean dynamics impact on the contrasting sea-ice trends around West Antarctica. *Journal of Geophysical Research: Oceans*, *122*(5), 4413–4430. https://doi.org/10.1002/2016JC012416

Le Grix, N., Burger, F. A., & Frölicher, T. L. (2025). Surface and subsurface compound marine heatwave and biogeochemical extremes under climate change. *Global Biogeochemical Cycles*, *39*(5), e2025GB008514. https://doi.org/10.1029/2025GB008514

Leseurre, C., Lo Monaco, C., Reverdin, G., Metzl, N., Fin, J., Mignon, C., & Benito, L. (2022). Summer trends and drivers of sea surface fCO_2 and pH changes observed in the southern Indian Ocean over the last two decades (1998–2019). *Biogeosciences*, *19*(10), 2599–2625. https://doi.org/10.5194/bg-19-2599-2022

L'Heureux, M. L., & Thompson, D. W. J. (2006). Observed relationships between the El Niño–Southern Oscillation and the extratropical zonal-mean circulation. *Journal of Climate*, *19*(2), 276–287. https://doi.org/10.1175/JCLI3617.1

Liu, W., Liu, Z., & Li, S. (2021). The driving mechanisms on Southern Ocean upwelling change during the last deglaciation. *Geosciences*, *11*(7), 266. https://doi.org/10.3390/geosciences11070266

Loose, B., & Schlosser, P. (2011). Sea ice and its effect on CO_2 flux between the atmosphere and the Southern Ocean interior. *Journal of Geophysical Research*, *116*(C11). https://doi.org/10.1029/2010JC006509

Lovecchio, E., Clément, L., Evans, C., Rayne, R., Dumousseaud, C., Roshan, S., et al. (2023). Export of Dissolved Organic Carbon (DOC) compared to the particulate and active fluxes near South Georgia, Southern Ocean. *Deep Sea Research Part II: Topical Studies in Oceanography*, *212*, 105338. https://doi.org/10.1016/j.dsr2.2023.105338

Lovenduski, N. S., Gruber, N., Doney, S. C., & Lima, I. D. (2007). Enhanced CO_2 outgassing in the Southern Ocean from a positive phase of the southern annular mode. *Global Biogeochemical Cycles*, *21*(2). https://doi.org/10.1029/2006GB002900

Lowe, A. T., Ross, R. M., Quetin, L. B., Vernet, M., & Fritsen, C. H. (2012). Simulating larval Antarctic krill growth and condition factor during fall and winter in response to environmental variability. *Marine Ecology Progress Series*, *452*, 27–43. https://doi.org/10.3354/meps09409

MacQueen, J. (1967). Some methods for classification and analysis of multivariate observations. *Proceedings of the fifth Berkeley symposium on mathematical statistics and probability*, *1*, 281–297.

Malan, N., Gupta, A. S., Schaeffer, A., Zhang, S., Doblin, M. A., Pilo, G. S., et al. (2025). Lifting the lid on marine heatwaves. *Progress in Oceanography*, *239*, 103539. https://doi.org/10.1016/j.pocean.2025.103539

Marschall, H.-P. (1988). The overwintering strategy of Antarctic krill under the pack-ice of the Weddell Sea. *Polar Biology*, *9*(2), 129–135. https://doi.org/10.1007/BF00442041

Marshall, J., & Speer, K. (2012). Closure of the meridional overturning circulation through Southern Ocean upwelling. *Nature Geoscience*, *5*(3), 171–180. https://doi.org/10.1038/ngeo1391

Montie, S., Thomsen, M. S., Rack, W., & Broady, P. A. (2020). Extreme summer marine heatwaves increase chlorophyll a in the Southern Ocean. *Antarctic Science*, *32*(6), 508–509. https://doi.org/10.1017/S0954102020000401

Moore, J. K., Lindsay, K., Doney, S. C., Long, M. C., & Misumi, K. (2013). Marine ecosystem dynamics and biogeochemical cycling in the community earth system model [CESM1(BGC)]: Comparison of the 1990s with the 2090s under the RCP4.5 and RCP8.5 scenarios. *Journal of Climate*, *26*(23), 9291–9312. https://doi.org/10.1175/JCLI-D-12-00566.1

Moreau, S., Penna, A. D., Llort, J., Patel, R., Langlais, C., Boyd, P. W., et al. (2017). Eddy-induced carbon transport across the Antarctic circumpolar current. *Global Biogeochemical Cycles*, *31*(9), 1368–1386. https://doi.org/10.1002/2017GB005669

Morrison, A. K., Frölicher, T. L., & Sarmiento, J. L. (2015). Upwelling in the Southern Ocean. *Physics Today*, *68*(1), 27–32. https://doi.org/10.1063/PT.3.2654

Morrison, A. K., Hogg, A. M., England, M. H., & Spence, P. (2020). Warm Circumpolar Deep Water transport toward Antarctica driven by local dense water export in canyons. *Science Advances*, *6*(18), eaav2516. https://doi.org/10.1126/sciadv.aav2516

Nakayama, Y., Menemenlis, D., Zhang, H., Schodlok, M., & Rignot, E. (2018). Origin of Circumpolar Deep Water intruding onto the Amundsen and Bellingshausen Sea Continental shelves. *Nature Communications*, *9*(1), 3403. https://doi.org/10.1038/s41467-018-05813-1

NOAA. (n.d.). Cold & Warm episodes by season. Retrieved from https://www.cpc.ncep.noaa.gov/products/analysis_monitoring/ensostuff/ONI_v5.php

Olbers, D., Borowski, D., Völker, C., & Wölff, J.-O. (2004). The dynamical balance, transport and circulation of the Antarctic circumpolar current. *Antarctic Science*, *16*(4), 439–470. https://doi.org/10.1017/S0954102004002251

Oliver, E. C., Benthuysen, J. A., Darmaraki, S., Donat, M. G., Hobday, A. J., Holbrook, N. J., et al. (2021). Marine heatwaves. *Annual Review of Marine Science*, *13*(1), 1–30. https://doi.org/10.1146/annurev-marine-032720-095144

Orr, J. C., & Epitalon, J. M. (2015). Improved routines to model the ocean carbonate system: Mocsy 2.0. *Geoscientific Model Development*, *8*(3), 485–499. https://doi.org/10.5194/gmd-8-485-2015

Pellichero, V., Sallée, J.-B., Schmidtko, S., Roquet, F., & Charrassin, J.-B. (2017). The ocean mixed layer under Southern Ocean sea-ice: Seasonal cycle and forcing. *Journal of Geophysical Research: Oceans*, *122*(2), 1608–1633. https://doi.org/10.1002/2016JC011970

Pinkerton, M. H., Boyd, P. W., Deppeler, S., Hayward, A., Höfer, J., & Moreau, S. (2021). Evidence for the impact of climate change on primary producers in the Southern Ocean. *Frontiers in Ecology and Evolution*, *9*, 592027. https://doi.org/10.3389/fevo.2021.592027

Quetin, L. B., & Ross, R. M. (2009). Life under Antarctic pack ice: A krill perspective. In *Smithsonian at the poles: Contributions to international polar year science* (pp. 285–298). IPY. https://doi.org/10.5479/si.097884601X.21

Ramadhan, A., Marshall, J., Meneghello, G., Illari, L., & Speer, K. (2022). Observations of upwelling and downwelling around Antarctica mediated by sea ice. *Frontiers in Marine Science*, *9*, 864808. https://doi.org/10.3389/fmars.2022.864808

Richaud, B., Hu, X., Darmaraki, S., Fennel, K., Lu, Y., & Oliver, E. C. J. (2024). Drivers of marine heatwaves in the Arctic Ocean. *Journal of Geophysical Research: Oceans*, *129*(2), e2023JC020324. https://doi.org/10.1029/2023JC020324

Sala, J., Giglio, D., Capotondi, A., Sukianto, T., & Kuusela, M. (2025). Leading dynamical processes of global marine heatwaves in an ocean state estimate. *Ocean Science*, *21*(5), 2463–2479. https://doi.org/10.5194/os-21-2463-2025

19449224, 2026, 10, Downloaded from https://agupubs.onlinelibrary.wiley.com/doi/10.1029/2026GB009430 by Catherine Becker - University Of Southampton , Wiley Online Library on [11/11/2026]. See the Terms and Conditions (https://onlinelibrary.wiley.com/terms-and-conditions) on Wiley Online Library for rules of use; OA articles are governed by the applicable Creative Commons License

Sarmiento, J. L., & Gruber, N. (2006). *Ocean biogeochemical dynamics*. Princeton University Press. https://doi.org/10.2307/j.ctt3fgxqx
Schaeffer, A., & Roughan, M. (2017). Subsurface intensification of marine heatwaves off southeastern Australia: The role of stratification and local winds. *Geophysical Research Letters*, *44*(10), 5025–5033. https://doi.org/10.1002/2017GL073714
Schlegel, R. W., Oliver, E. C. J., & Chen, K. (2021). Drivers of marine heatwaves in the northwest Atlantic: The role of air–sea interaction during onset and decline. *Frontiers in Marine Science*, *8*, 627970. https://doi.org/10.3389/fmars.2021.627970
Schmidt, K., Atkinson, A., Pond, D. W., & Ireland, L. C. (2014). Feeding and overwintering of Antarctic krill across its major habitats: The role of sea ice cover, water depth, and phytoplankton abundance. *Limnology and Oceanography*, *59*(1), 17–36. https://doi.org/10.4319/lo.2014.59.1.0017
Sen Gupta, A., Thomsen, M., Benthuysen, J. A., Hobday, A. J., Oliver, E., Alexander, L. V., & Smale, D. A. (2020). Drivers and impacts of the most extreme marine heatwaves events. *Scientific Reports*, *10*(1), 1–15. https://doi.org/10.1038/s41598-020-75445-3
Sen Gupta, A. S., & England, M. H. (2006). Coupled ocean–atmosphere–ice response to variations in the southern annular mode. *Journal of Climate*, *19*(18), 4457–4486. https://doi.org/10.1175/JCLI3843.1
Shchepetkin, A. F., & McWilliams, J. C. (2005). The regional oceanic modeling system (ROMS): A split-explicit, free-surface, topography-following-coordinate oceanic model. *Ocean Modelling*, *9*(4), 347–404. https://doi.org/10.1016/j.ocemod.2004.08.002
Smith, K. E., Sen Gupta, A., Amaya, D., Benthuysen, J. A., Burrows, M. T., Capotondi, A., et al. (2025). Baseline matters: Challenges and implications of different marine heatwave baselines. *Progress in Oceanography*, *231*, 103404. https://doi.org/10.1016/j.pocean.2024.103404
Spillman, C. M., Smith, G. A., Hobday, A. J., & Hartog, J. R. (2021). Onset and decline rates of marine heatwaves: Global trends, seasonal forecasts and marine management. *Frontiers in Climate*, *3*, 801217. https://doi.org/10.3389/fclim.2021.801217
Stuecker, M. F., Bitz, C. M., & Armour, K. C. (2017). Conditions leading to the unprecedented low Antarctic sea ice extent during the 2016 austral spring season. *Geophysical Research Letters*, *44*(17), 9008–9019. https://doi.org/10.1002/2017GL074691
Sun, Y., & Ellwood, M. J. (2025). Calcium carbonate cycling in the Southern Ocean: Insights from dissolved calcium and potential alkalinity tracers. *Limnology and Oceanography Letters*, *10*(2), 254–263. https://doi.org/10.1002/lol2.10457
Taylor, J. R., Bachman, S., Stamper, M., Hosegood, P., Adams, K., Sallee, J.-B., & Torres, R. (2018). Submesoscale Rossby waves on the Antarctic circumpolar current. *Science Advances*, *4*(3), eaao2824. https://doi.org/10.1126/sciadv.aao2824
Thompson, A. F. (2008). The atmospheric ocean: Eddies and jets in the Antarctic circumpolar current. *Philosophical Transactions of the Royal Society A: Mathematical, Physical and Engineering Sciences*, *366*(1885), 4529–4541. https://doi.org/10.1098/rsta.2008.0196
Wang, G., Cai, W., Santoso, A., Wu, L., Fyfe, J. C., Yeh, S.-W., et al. (2022). Future Southern Ocean warming linked to projected ENSO variability. *Nature Climate Change*, *12*(7), 649–654. https://doi.org/10.1038/s41558-022-01398-2
Wang, J., Luo, H., Yu, L., Li, X., Holland, P. R., & Yang, Q. (2023). The impacts of combined SAM and ENSO on seasonal Antarctic sea ice changes. *Journal of Climate*, *36*(11), 3553–3569. https://doi.org/10.1175/JCLI-D-22-0679.1
Wang, Z., Turner, J., Wu, Y., & Liu, C. (2019). Rapid decline of total Antarctic sea ice extent during 2014–16 controlled by wind-driven sea ice drift. *Journal of Climate*, *32*(17), 5381–5395. https://doi.org/10.1175/JCLI-D-18-0635.1
Wilson, E. A., Riser, S. C., Campbell, E. C., & Wong, A. P. (2019). Winter upper-ocean stability and ice-ocean feedbacks in the sea ice-covered Southern Ocean. *Journal of Physical Oceanography*, *49*(4), 1099–1117. https://doi.org/10.1175/JPO-D-18-0184.1
Wong, J., Münnich, M., & Gruber, N. (2024). Column-compound extremes in the global ocean. *AGU Advances*, *5*(3), e2023AV001059. https://doi.org/10.1029/2023AV001059
Wong, J., Münnich, M., & Gruber, N. (2025). Compound marine heatwaves and acidity extremes in the Southern Ocean. *Global Biogeochemical Cycles*, *39*(10), e2025GB008630. https://doi.org/10.1029/2025GB008630
Wong, J., Münnich, M., & Gruber, N. (2026). Drivers of compound marine heatwaves and acidity extremes in the Southern Ocean [Dataset]. *ETH Research Collection*. https://doi.org/10.3929/ethz-c-000802906
Zhang, Y., Du, Y., Feng, M., & Hobday, A. J. (2023). Vertical structures of marine heatwaves. *Nature Communications*, *14*(1), 6483. https://doi.org/10.1038/s41467-023-42219-0
Zwally, H. J., Comiso, J. C., Parkinson, C. L., Cavalieri, D. J., & Gloersen, P. (2002). Variability of Antarctic sea ice 1979–1998. *Journal of Geophysical Research*, *107*(C5). https://doi.org/10.1029/2000JC000733

19449224, 2026, 10, Downloaded from https://agupubs.onlinelibrary.wiley.com/doi/10.1029/2026GB009430 by Catherine Becker - University Of Southampton , Wiley Online Library on [11/11/2026]. See the Terms and Conditions (https://onlinelibrary.wiley.com/terms-and-conditions) on Wiley Online Library for rules of use; OA articles are governed by the applicable Creative Commons License